A Spatio-Temporal Understanding of Growth Regulation during the Salt Stress Response in *Arabidopsis*[W]

Yu Geng,[a,b,c,1] Rui Wu,[a,b,c,1] Choon Wei Wee,[b,1] Fei Xie,[b] Xueliang Wei,[a] Penny Mei Yeen Chan,[b,c] Cliff Tham,[b] Lina Duan,[a,b,c] and José R. Dinneny[a,b,c,2]

[a] Carnegie Institution for Science, Department of Plant Biology, Stanford, California 94305
[b] Temasek Lifesciences Laboratory, National University of Singapore, Singapore, 117604, Singapore
[c] Department of Biological Sciences, National University of Singapore, Singapore, 117543, Singapore

ORCID IDs: 000-0002-2348-8059 (R.W.); 0000-0002-3998-724X (J.R.D.).

Plant environmental responses involve dynamic changes in growth and signaling, yet little is understood as to how progress through these events is regulated. Here, we explored the phenotypic and transcriptional events involved in the acclimation of the *Arabidopsis thaliana* seedling root to a rapid change in salinity. Using live-imaging analysis, we show that growth is dynamically regulated with a period of quiescence followed by recovery then homeostasis. Through the use of a new high-resolution spatio-temporal transcriptional map, we identify the key hormone signaling pathways that regulate specific transcriptional programs, predict their spatial domain of action, and link the activity of these pathways to the regulation of specific phases of growth. We use tissue-specific approaches to suppress the abscisic acid (ABA) signaling pathway and demonstrate that ABA likely acts in select tissue layers to regulate spatially localized transcriptional programs and promote growth recovery. Finally, we show that salt also regulates many tissue-specific and time point–specific transcriptional responses that are expected to modify water transport, Casparian strip formation, and protein translation. Together, our data reveal a sophisticated assortment of regulatory programs acting together to coordinate spatially patterned biological changes involved in the immediate and long-term response to a stressful shift in environment.

INTRODUCTION

Multicellular organisms are composed of complex assortments of tissues and cell types that must coordinate biological activities to enable survival. Through recent studies, the root of *Arabidopsis thaliana* has become an informative model organ system for dissecting the response of plants to changes in the environment (Dinneny and Benfey, 2009; Dinneny, 2013). The *Arabidopsis* root is essentially composed of concentric layers of different tissue types surrounding a central core of stele tissue where the vasculature is housed (Scheres et al., 2002). Currently, several methodologies have been developed that enable the profiling of cell type–specific biological information in this organ (Birnbaum et al., 2005; Mustroph et al., 2009; Wee and Dinneny, 2010; Deal and Henikoff, 2011). The most widely applied method uses fluorescence-activated cell sorting (FACS) of cells after a brief protoplasting treatment of roots expressing tissue-specific green fluorescent protein (GFP) reporters (Birnbaum et al., 2003, 2005). This method has been used to characterize the transcriptome of nearly every cell type in the root and has provided an important resource for studies in developmental biology, signal transduction, and physiology (Birnbaum et al., 2003; Nawy et al., 2005; Lee et al., 2006; Brady et al., 2007;

Sozzani et al., 2010). In addition to transcript profiling, deep sequencing of small RNAs, hormone quantitation, and proteomic and metabolomic analyses have also been performed on FACS-isolated cells, illustrating the tremendous versatility of the method and the validity of the biological information generated (Petersson et al., 2009; Breakfield et al., 2012; Petricka et al., 2012; Rogers et al., 2012).

Nonstressful growth conditions are useful for understanding cellular processes at steady state levels or processes that change over developmental time. In nature, however, roots will encounter a constantly changing environment due to the heterogeneity of soil. As such, displacement of the root tip, through growth, leads to a constant flux of encountered environmental conditions that require the regulation of context appropriate acclimatory mechanisms. FACS has proven useful for exploring the response of root tissues to changes in abiotic conditions, such as nitrogen content (Gifford et al., 2008), high salinity (Dinneny et al., 2008), low pH (Iyer-Pascuzzi et al., 2011), and nutrient deprivation conditions (low iron or low sulfur) (Dinneny et al., 2008; Iyer-Pascuzzi et al., 2011). Meta-analyses of these data has shown that each environmental condition targets a distinct set of tissue layers in the root and regulates changes in transcriptional states that affect growth and physiology (Dinneny et al., 2008; Iyer-Pascuzzi et al., 2011).

High salinity is an important agricultural contaminant that causes damage to the plant, in part, through ionic and osmotic stress (Flowers et al., 1997; Munns, 2002; Xiong and Zhu, 2002). Sodium chloride (NaCl) elicits rapid and dynamic changes in gene expression, which overlap with responses to the hormone abscisic acid (ABA) (Zhu, 2002; Fujita et al., 2011). ABA biosynthesis

increases under salt stress conditions and can mediate growth suppression (Finkelstein and Rock, 2002; Achard et al., 2006). In the root, NaCl has been shown to stabilize REPRESSOR OF GA1 (RGA1), a growth-repressing DELLA protein, and this effect is dependent upon ABA signaling (Achard et al., 2006). Water stress elicits many similar responses as high salinity, and several studies in maize (*Zea mays*) and tomato (*Solanum lycopersicum*) have shown that ABA can also have growth promoting activity in the root and shoot by limiting ethylene biosynthesis, which is activated under water stress (Sharp et al., 2000; Spollen et al., 2000; Sharp and LeNoble, 2002). The role of ABA in this context is quite intriguing, as ABA activates growth at low levels and represses it at moderate to high levels under normal conditions (Finkelstein and Rock, 2002). When and where these signals act to regulate growth and if these responses are dynamically regulated during acclimation are not fully understood.

Studies using time-lapse imaging have begun to transform the analysis of growth and signaling in plants (Miller et al., 2007; Reddy et al., 2007). Live imaging enables a more complete understanding of the changes that occur during environmental flux. Analysis of gravitropism in seeds of varying size (Brooks et al., 2010) and light-regulated hypocotyl growth in mutants (Miller et al., 2007; Wu et al., 2010) have revealed subtle, yet significant alterations that would be difficult, if not impossible, to detect using measurements of growth at an arbitrary end point. These studies have also identified phases of the response, which suggest the occurrence of important regulatory events. Recent work examining osmotic stress responses in the shoot have highlighted the dynamic nature of the acclimation process (Skirycz et al., 2010, 2011). Upon treatment of seedlings with mannitol, an osmotic stress simulant, leaves exhibit temporally dynamic changes in gene expression and growth. These changes are dependent upon the developmental stage of the leaf and the length of treatment. Temporally regulated fluctuations in hormone signaling are thought to play a major role in regulating these events.

Here, we describe an in-depth investigation of growth regulation in the *Arabidopsis* root during the salt stress response. Using live imaging, we reveal that salt stress induces a brief period of quiescence followed by growth recovery. To identify the key signaling pathways regulating such dynamics and to understand the broader impact of salt stress at the spatio-temporal level, we generated a tissue-specific, multi–time point global transcriptional data set. Gene expression was examined in two control conditions and at six time points between 1 and 48 h after salt treatment. These data provide a highly resolved resource that enables the use of spatial and temporal trends to generate hypotheses regarding the regulation of these expression patterns.

Environmental responses in plants are regulated, in part, through a complex secondary signaling network enacted by changes in hormone biosynthesis (Dinneny et al., 2008; Iyer-Pascuzzi et al., 2011). To deconvolve this signaling network, we developed a bioinformatic method that uses publically available hormone response data sets to identify the pathways that regulate specific downstream salt-regulated expression patterns. We directly test the function of these pathways in growth regulation using mutants or chemical inhibitors that disrupt the biosynthesis or signal transduction of these hormones. The use

of tissue-specific strategies for the manipulation of ABA signaling revealed a particularly important role for inner tissue layers in regulating ABA-mediated salt stress transcriptional responses. We confirmed the importance of such signaling in growth regulation using live-imaging analysis. Together, our study provides a highly resolved understanding of the regulatory networks that generate the complex spatio-temporal expression patterns occurring during a stress response and an understanding of dynamic growth regulation. Based on these results, we propose that the dynamic regulation of growth and gene expression is a result of phasic shifts in the biosynthesis and signaling of multiple plant hormones that stimulate or repress growth.

RESULTS

Growth Regulation by Salt Stress Is a Multi-Phasic Process

Upon exposure of plants to an immediate change in salinity (salt shock), rapid and dynamic changes in the growth of the root and shoot have been observed (Rodríguez et al., 1997; Passioura and Munns, 2000; Munns, 2002). These initial changes in growth are driven by the osmotic component of salt stress, which immediately affects the water status of the plant, preventing cell elongation. Within several hours after treatment, partial recovery of growth occurs and is due to the uptake of inorganic ions and the synthesis of compatible osmolytes, which reduce the water potential of the cell until cell expansion can resume.

We wanted to determine whether the primary root of *Arabidopsis* seedlings exhibited similar dynamic changes in growth after salinity treatment with the ultimate goal of identifying the regulatory pathways that enable growth recovery. We utilized a custom live-imaging system, in which seedlings were grown vertically on the surface of agar in tissue culture plates and imaged using transmitted infrared light (see Supplemental Figure 1A online) (Duan et al., 2013). Our imaging system uses a computer-controlled rotating stage with six plate holders enabling the simultaneous imaging of roots grown under different environmental conditions. Images were captured once every 15 min and root growth quantified using semiautomated image analysis software we developed that enables the measurement of growth independent of the effects of root tip waving (see Supplemental Figures 1B to 1E, Supplemental Data Set 1, and Supplemental Movie 1 online).

Columbia-0 (Col-0) seedlings were first grown for 5 d under standard conditions and then transferred back to fresh medium or to medium supplemented with 140 mM NaCl. This concentration of salt was previously shown to substantially inhibit root growth but does not cause seedling death (Dinneny et al., 2008). Roots transferred to standard conditions showed a slight suppression of growth, presumably due to the effects of being physically transferred, which was followed immediately by growth recovery (Figures 1A and 1B; see Supplemental Movie 2 online). Salt-treated roots showed a much more dynamic and severe change in growth rate (Figures 1A and 1B). During the first 4 to 5 h of treatment, growth rates fell (stop phase). Slow growth was then maintained for ~4 h (quiescent phase). Quiescence was followed by a period of growth recovery occurring between 8 and 13 h after transfer (recovery phase). Finally, stabilization of growth rates
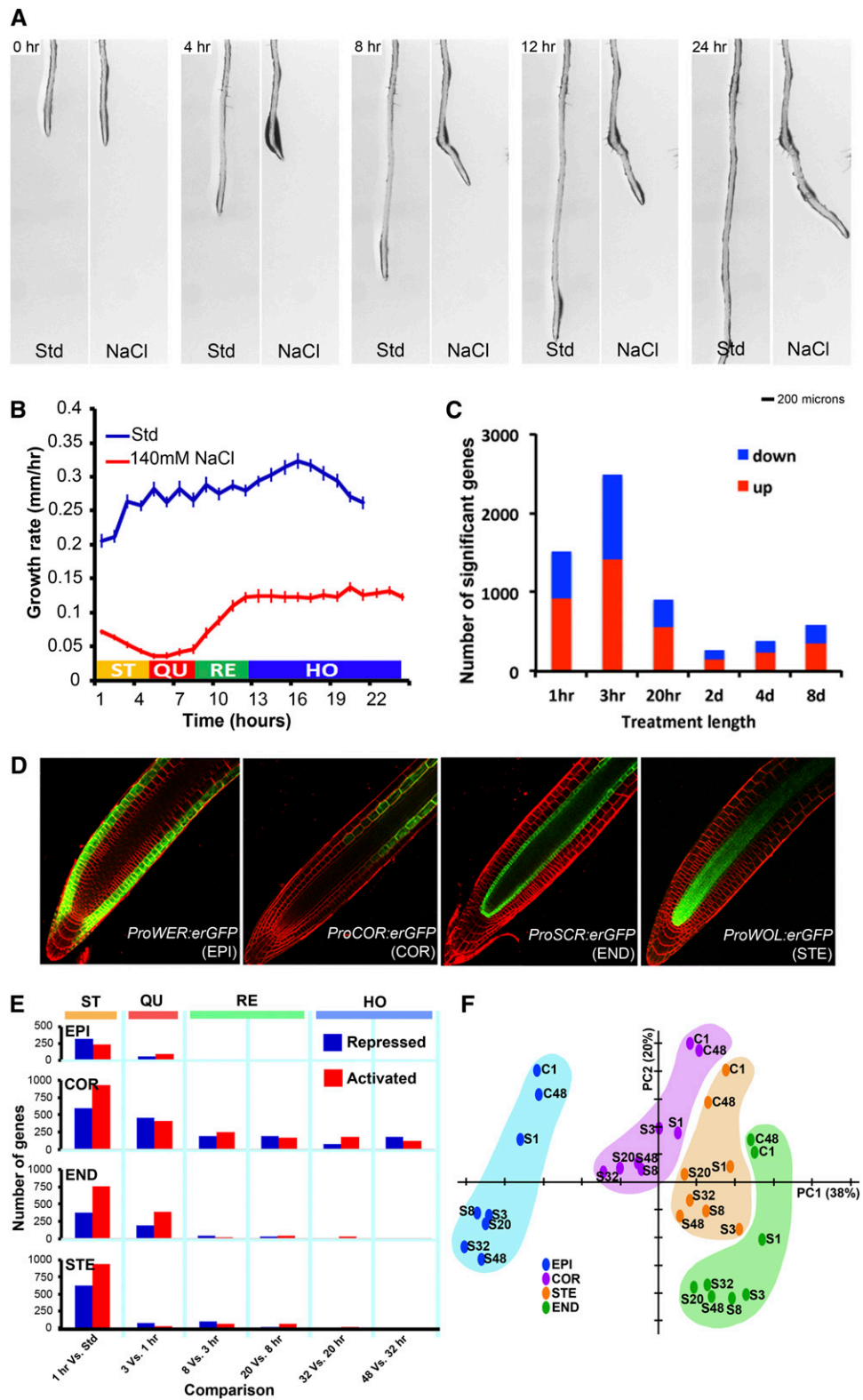
Figure 1. Salt Treatment Caused Dynamic Changes in Growth: Generation of a Spatio-Temporal Gene Expression Map of the Response.

(A) Time-lapse images of roots after transfer to standard conditions or medium supplemented with 140 mM NaCl. Bar = 200 μm.

occurred between 13 and 24 h after transfer (homeostasis phase). These data showed that salt stress did not simply cause steady state growth rates to decrease; there were discrete phases where growth was strongly suppressed and other phases where growth rates actually increased. The different rates of growth and times at which growth rates changed suggested to us that the salt response is regulated by a temporally dynamic regulatory process that may involve distinct signaling events.

Generation of a Spatio-Temporal Global Transcriptional Map of the Salt Stress Response

In our prior studies examining the response of roots to salt stress, we transcriptionally profiled six tissue layers isolated from roots grown under standard conditions and roots transferred to medium supplemented with 140 mM NaCl for 1 h (Dinneny et al., 2008; Dinneny, 2010). This data set provided a snapshot of the transcriptional regulation that occurs in the different tissue layers of the root and revealed the extensive tissue specificity of the response. However, results in that study and the observations we have made here using live imaging indicated that the response of the root to salt is temporally dynamic and that additional transcriptional programs are elicited at later time points. To characterize these dynamic programs and determine what role tissue-specific regulatory pathways play, we decided to generate a spatio-temporal transcriptional map of the salt stress response that spanned the various phases of growth we observed through live imaging.

To examine at what time transcriptional homeostasis occurs in the root, we performed microarray-based transcriptional profiling of whole roots transferred to salt stress conditions for prolonged periods of time ranging from 1 h to 8 d. Roots were also transferred to standard medium and expression analyzed to determine the effects of physical transfer and to test for the effects of seedling developmental age in this extended time-course analysis. To avoid the effects of circadian rhythm on gene expression patterns, roots were transferred to treatment conditions in a staggered fashion so that harvesting of tissue occurred at the same time of day.

We found that the largest fraction of transcriptional changes occurred during the first 24 h (76.1% of all significantly differentially expressed genes) with 3 h of salt treatment being the most responsive time point (40.4% of responding genes), which is similar to the time of peak transcriptional activity observed before (Figure 1C; see Supplemental Data Set 2 online) (Dinneny

et al., 2008). A relatively low level of transcriptional fluctuations marked later time points and indicated that transcriptional homeostasis occurred between 24 and 48 h after salt treatment. These data showed that the extent of transcriptional regulation correlated well with the occurrence of phenotypic changes we observed. Analysis of Gene Ontology (GO) annotations in salt-regulated genes revealed that the large majority of annotations were enriched between the 1- to 48-h period (78.3%; see Supplemental Figure 2 and Supplemental Data Set 2 online) (Ashburner, 2000). Analysis of the control time points revealed that few genes were differentially expressed over developmental age (see Supplemental Data Set 2 online). Comparisons between the 8-d and 1- or 3-h control time points identified the majority of differentially expressed genes (449 and 282 genes, respectively), while other comparison showed few if any significant differences.

Based on these whole-root profiling results, we defined the temporal boundaries of our spatio-temporal transcriptional map to be comprised of time points between 1 and 48 h of salinity treatment. Root samples were harvested from seedlings treated with salt for 1, 3, 8, 20, 32, or 48 h. In addition, two control conditions were used (transfer to standard conditions for 1 or 48 h). Controls were not performed at every time point as our whole root analyses indicated that no significant transcriptional differences were detected between control time points before 48 h of growth on standard conditions (Figure 1D; P value < 0.001).

Four different GFP-based reporter lines were used for FACS isolation of specific cell/tissue types (Figure 1D). The *ProWEREWOLF:erGFP* reporter marks cells of the lateral root cap and epidermis, including trichoblast and atrichoblast cells in the meristematic region of the root (abbreviated as EPI) (Lee and Schiefelbein, 1999). The *ProCORTEX:erGFP* reporter marks cells of the cortex except in the proximal meristematic zone (abbreviated as COR) (Lee et al., 2006). *ProSCARECROW:erGFP* was used to isolate cells of the quiescent center and endodermis (abbreviated as END) (Sabatini et al., 2003; Dinneny et al., 2008), while the *ProWOODENLEG:erGFP* reporter allowed isolation of stele cells, which include the pericycle and vascular cell types (abbreviated as STE) (Helariutta et al., 2000). These GFP reporter lines were examined after different periods of salt treatment, and no significant changes in the cell-type specificity of the expression patterns were observed (see Supplemental Figure 3 online).

FACS isolated cell populations were examined by fluorescence microscopy to verify enrichment of GFP-positive cells

Figure 1. (continued).

(B) Quantification of growth rates for roots transferred to standard (n = 16) or 140 mM NaCl (n = 30) conditions. Note that salt induced dynamic changes in growth rates not observed under standard conditions. ST, stop phase; QU, quiescence phase; RE, recovery phase; HO, homeostasis phase.
(C) Number of genes with a significant increase or decrease in expression at different time points after transfer to salt stress as determined by transcriptional profiling of whole roots.
(D) Confocal images of *ProWER:erGFP*, *ProCOR:erGFP*, *ProSCR:erGFP*, and *ProWOL:erGFP*, which were used in the FACS isolation of specific cell layers in this study. GFP fluorescence (green; bright) shows reporter activity, and FM4-64 is used as a counterstain (red).
(E) Number of genes that showed differential expression at different time points and in each cell layer after salt treatment.
(F) Principal component analysis of the different sample types composing the spatio-temporal map of the salt response. C, control conditions, S, salt stress conditions.
Growth data are presented as a percentage of difference in growth rate relative to standard conditions. Error is SE.

(see Supplemental Figure 4 online). On average, 85% of cells isolated by FACS expressed GFP, which is higher than the enrichment level reported in another study (Deal and Henikoff, 2010). RNA was isolated, processed, and hybridized to Affymetrix ATH1 microarrays to obtain expression profiles for over 21,000 nuclear encoded transcripts (see Supplemental Data Set 3 online). The 1- and 48-h control treatments were compared with each other for each cell type using LIMMA (for Linear Models of Microarray Data) to identify genes whose expression pattern changed due to developmental age (see Supplemental Data Set 3 online) (Smyth, 2005).

To identify genes whose expression changed during the salt response in each cell type, we performed pairwise statistical tests between subsequent time points (e.g., standard 1 h versus NaCl 1 h, NaCl 1 h versus NaCl 3 h, etc.) for each cell type using LIMMA and identified 4344 significantly differentially expressed genes (Figure 1E; see Supplemental Data Set 4 online) (Smyth, 2005). Genes identified using this analysis were combined with a list of significant differentially expressed genes identified using a time course–specific statistical package, EDGE, which models temporal data as splines to take advantage of the nonindependent nature of samples collected over time (default cutoff of 10% false discovery rate and twofold change criteria used to identify 2996 differentially expressed genes; see Supplemental Data Set 4 online) (Storey et al., 2005; Leek et al., 2006). For each cell type, we excluded from our list of significant salt-regulated genes those that were also significantly regulated by developmental age. Based on this analysis pipeline, we generated a combined list of 5590 genes we considered salt regulated (see Supplemental Data Set 4 online). We tested a set of six salt-regulated genes by quantitative RT-PCR (qRT-PCR) and found that their temporal profiles correlated well with the expression profiles generated by microarray analysis (see Supplemental Figure 5 online). A set of 28 genes with known tissue-specific expression was examined in our data set, and all but two showed peak expression in the expected tissue layer, indicating a high degree of spatial accuracy in our data set (see Supplemental Figure 6 online). To visualize the spatio-temporal changes in gene expression patterns, an eFP-style (electronic fluorescence pictograph) representation was used to illustrate expression of a single gene in each cell type under all conditions profiled (Figures 2C to 2J) (Winter et al., 2007).

We characterized the cell-type specificity of our salt-responsive gene list and found that, at every time point, the largest portion of transcriptional changes occurred in single cell types (see Supplemental Figure 7 online). Similar to our previous findings (Dinneny et al., 2008), the COR cell layer was the most transcriptionally active cell layer throughout the time course (Figure 1E). Principal component analysis of the spatio-temporal map was performed to find associations between the various cell types and time points. Based on the first two principal components (58% of variation captured), we found that the relative relationship between the transcriptional profiles of each cell type with respect to the other cell types, was maintained throughout the salt stress response (Figure 1F). This indicates that cell types maintained their transcriptional distinctions despite tremendous fluctuations in transcriptional state.

Predominant Expression Patterns Highlight Both Autonomy and Coordination in the Stress Response of Each Cell Layer

Salt-regulated genes were organized into 25 coexpressed clusters using the fuzzy C-means algorithm (Figure 2A; see Supplemental Data Set 5 online) (Hathaway et al., 1996). We utilized algorithm settings that only incorporated genes into clusters if their correlation to the centroid was high, which resulted in 3896 genes being clustered. GO term enrichment analysis was performed on each cluster to identify 200 (P value < 0.001) enriched biological functions present in this data set (Figure 2B; see Supplemental Data Set 5 online). A survey of the expression patterns represented in these clusters revealed several modes of transcriptional regulation distinguished by the level of cell-type specificity and temporal dynamism of the transcriptional response. For example, cluster 6 showed highly coordinated activation in gene expression across all cell types early in the salt response time course and was enriched for ABA-responsive genes (P value < 1E-8), such as *RESPONSIVE TO DESICCATION 29A* (*RD29A*) (Figure 2C). The early semiubiquitous activation of these ABA-responsive genes is consistent with the model proposed in our previous study that ABA and ABA-associated signaling is activated in all tissue layers of the root during the initial salt stress response (Dinneny et al., 2008). In other clusters, transcriptional responses that were coordinated between cell types also showed cell type–specific differences in the magnitude of change. For example cluster 8, which was enriched for genes encoding water channels (P value < 1E-7), showed a stable reduction in gene expression in all cell layers with a particularly strong reduction in the EPI layer (Figure 2D).

Other clusters showed more highly cell-type and time point–specific regulation. Cluster 3 showed peak expression in the END layer between 3 to 8 h after salt treatment (Figure 2E). This cluster was enriched for biological functions associated with Casparian strip formation, including suberin biosynthesis (P value < 1E-4) and laccase activity (P value < 1E-6), which is necessary for lignin biosynthesis (Naseer et al., 2012). Fluorol yellow staining of suberin in salt-treated roots confirmed the increased deposition of this compound during salt stress (see Supplemental Figure 8 online). In other species, the Casparian strip has been shown to enlarge during salt stress (Karahara et al., 2004) and may provide added protection against the absorption of sodium ions or act as a barrier to water loss.

Clusters 1 and 9 showed a steady increase in the expression of genes in the EPI and COR layers, peaking at 32 h; however, in the END and STE layers, salt activation was more moderate and peak expression in the STE layer was not observed until 48 h after salt treatment (Figures 2F and 2G). Clusters 1 and 9 had the largest number of gene members and showed particularly strong enrichment for genes associated with translation (cluster 1, P value < 1E-176; cluster 9, P value < 1E-7.6), ribosomal biogenesis (cluster 1, P value < 1E-61; cluster 9, P value < 1E-12) and rRNA processing (cluster 9, P value < 1E-10). Such transcriptional events suggested that late-phase growth recovery and homeostasis might be, in part, driven by an increase in the rate of protein translation.

Clusters 10, 19, and 21 exhibited highly dynamic and fluctuating expression patterns and contained genes associated with cell growth (Figures 2H to 2J). Cluster 10 showed coordinated
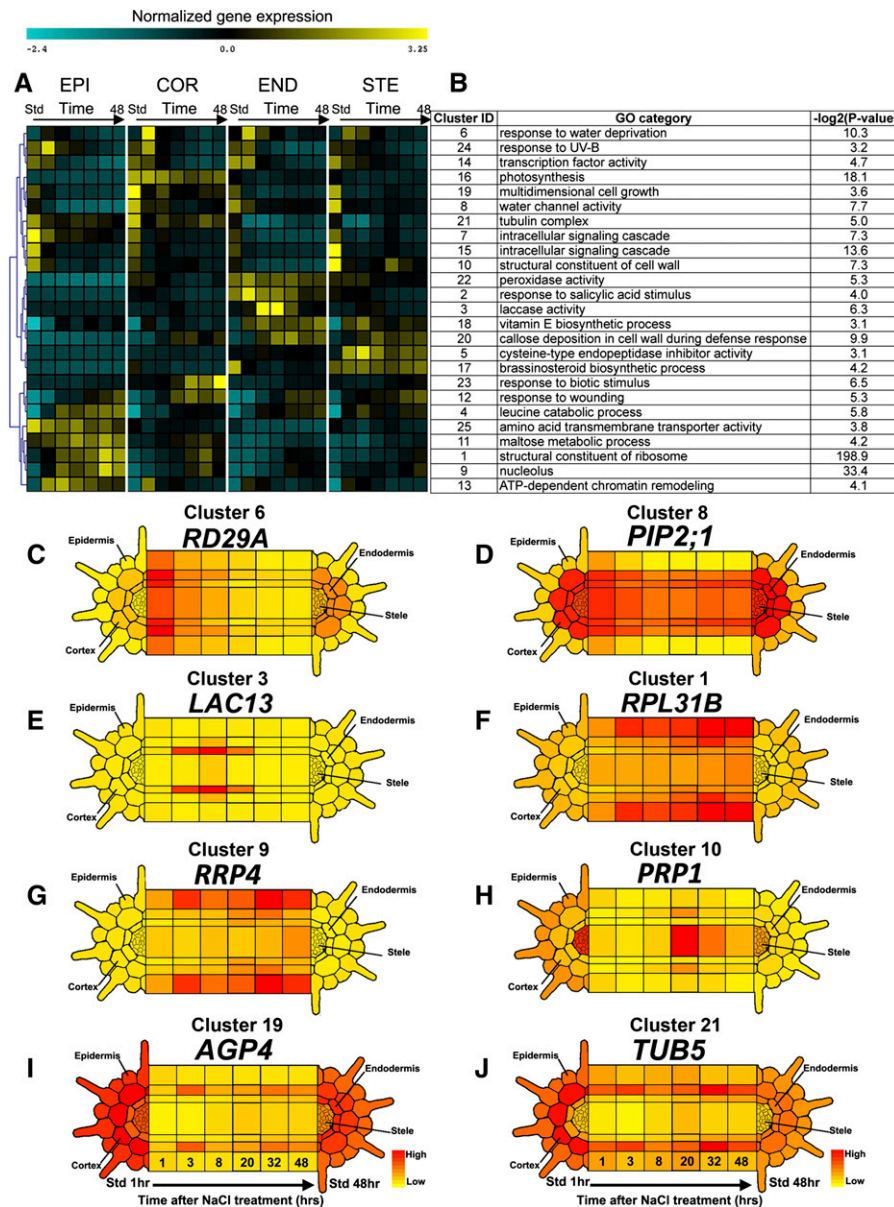
Normalized gene expression

−2.4   0.0   3.25

A

EPI   COR   END   STE

Std   Time   48 Std   Time   48 Std   Time   48 Std   Time   48

B

Cluster ID	GO category	-log2(P-value)
6	response to water deprivation	10.3
24	response to UV-B	3.2
14	transcription factor activity	4.7
16	photosynthesis	18.1
19	multidimensional cell growth	3.6
8	water channel activity	7.7
21	tubulin complex	5.0
7	intracellular signaling cascade	7.3
15	intracellular signaling cascade	13.6
10	structural constituent of cell wall	7.3
22	peroxidase activity	5.3
2	response to salicylic acid stimulus	4.0
3	laccase activity	6.3
18	vitamin E biosynthetic process	3.1
20	callose deposition in cell wall during defense response	9.9
5	cysteine-type endopeptidase inhibitor activity	3.1
17	brassinosteroid biosynthetic process	4.2
23	response to biotic stimulus	6.5
12	response to wounding	5.3
4	leucine catabolic process	5.8
25	amino acid transmembrane transporter activity	3.8
11	maltose metabolic process	4.2
1	structural constituent of ribosome	198.9
9	nucleolus	33.4
13	ATP-dependent chromatin remodeling	4.1

C Cluster 6 *RD29A*

D Cluster 8 *PIP2;1*

E Cluster 3 *LAC13*

F Cluster 1 *RPL31B*

G Cluster 9 *RRP4*

H Cluster 10 *PRP1*

I Cluster 19 *AGP4*

J Cluster 21 *TUB5*

1 3 8 20 32 48

Std 1hr → Std 48hr

High / Low

Time after NaCl treatment (hrs)

Figure 2. Spatio-Temporal Expression Patterns Observed during the Salt Response.

(A) Centroid profiles for each of the 25 gene clusters identified in the spatiotemporal data set.

(B) Select enriched GO categories for each cluster shown.

(C) to **(J)** eFP representation of expression for a collection of genes present in the various clusters described in the text.

(C) From cluster 6, At5g52310, *RD29A*.

(D) From cluster 22, At3g53420, PIP2;1.

(E) From cluster 3, At5g07130, *LACCASE13*.

(F) From cluster 1, At4g26230, 60S ribosomal protein L31.

(G) From cluster 9, At1g03360, *RRP4* (for *RRNA PROCESSING4*); RNA binding/exonuclease.

(H) From cluster 10, At1g54970, *PRP1* (for *PROLINE-RICH PROTEIN1*); structural constituent of cell wall.

(I) From cluster 19, At5g10430, *AGP4* (for *ARABINOGALACTAN PROTEIN4*).

(J) From cluster 21, At1g20010, *TUB5*; structural constituent of cytoskeleton.

downregulation in all cell layers early in the time course, and by 20 h, expression recovered in the EPI, COR, and STE layers but fell again by 48 h. This cluster was enriched for structural constituents of the cell wall (P value < 1E-7) and peroxidase activity (P value < 1E-6), which are both positively associated with growth (Figure 2H) (Arioli et al., 1998; Tsukagoshi et al., 2010). Clusters 19 (multidimensional cell growth, P-value < 1E-3) and 21 (tubulin complex, P value < 1E-5) also showed enrichment of other biological functions associated with growth (Figures 2I and 2J).

A Cluster Comparison Method Identifies Secondary Hormone Signaling Events during Salt Stress

Plant hormones are important intermediary signals regulating growth downstream of environmental stimuli. We wanted to develop a bioinformatic method that would allow us to identify which, if any, known hormone-signaling pathways might regulate root growth dynamics during salt stress and contribute to the various expression patterns we observed in our data set. Current methods for identifying targets of hormone signaling often use enrichment of GO annotations in gene lists. GO annotations, however, do not distinguish between transcriptional and posttranscriptional targets of a pathway. Hormones may also affect the expression of genes in a multiphasic manner, and GO annotations do not provide such resolution. The AtGenExpress consortium has generated data sets examining the temporal response of seedlings to various hormone treatments (Nemhauser et al., 2006; Kilian et al., 2007). These data provide a resource to identify subsets of genes that respond to hormone treatment in a coordinated manner and that represent submodules of the downstream transcriptional network. Such submodules are expected to have greater predictive power in identifying transcriptional programs that are affected by hormone signaling pathways.

We used LIMMA to identify genes differentially expressed in the AtGenExpress hormone treatment data sets and performed k-means clustering to segregate these genes into submodules based on their temporal response profiles (see Supplemental Data Set 6 online). Genes in these submodules were then analyzed for their membership in the set of 25 salt-responsive clusters we identified in the spatio-temporal map (Figure 2A; see Supplemental Data Set 6 online). The significance of the overlap in gene membership between each hormone submodule and each salt response cluster was tested using the hypergeometric distribution and corrected for multiple testing. A network diagram was drawn that included all hormone submodules and salt response clusters showing significant overlap (Q-value < 0.01) (Figure 3). The statistical significance of association between gene sets (nodes in the diagram) was indicated by the thickness of the edge between them. A repressive or activating arrowhead was drawn for edges based on the predicted regulatory role of the hormone signal on the salt-responsive cluster. For example, if a salt-responsive cluster was associated with a submodule where hormone treatment led to an increase in expression compared with the control, a positive-acting arrow was drawn. Our resulting secondary signaling network was composed of 13 salt-regulated clusters associated with 16 hormone submodules (Figure 3). ABA signaling was associated with the largest

number of salt-responsive clusters, six out of 13, followed by jasmonate (JA), four out of 13 (Figures 3A and 3B). These data suggested that ABA and JA may be responsible for regulating the greatest diversity of expression patterns in the root downstream of salt stress. Interestingly, brassinosteroid (BR) and gibberellic acid (GA) pathways, which have recently been shown to act synergistically to promote growth through direct protein–protein interaction of signaling pathway members (Bai et al., 2012; Gallego-Bartolomé et al., 2012), target the same set of salt-regulated clusters (19 and 21) (Figure 3C). Based on the results of our analysis, we chose to focus on ABA, JA, BR, and GA signaling during the salt stress response. Hormones such as ethylene (1-aminocyclopropane-1-carboxylic acid treatment used) and auxin (indole-3-acetic acid treatment used) were predicted to have relatively minor roles in the overall regulation of diverse transcriptional programs during salt stress and were not examined further.

ABA Signaling Is Associated with Broadly Regulated and Tissue-Specific Transcriptional Responses Distinguished by the Timing of Their Expression

Our inferred secondary signaling network suggested that ABA has the most diverse role in the regulation of transcriptional programs during salt stress (Figure 3A). Six salt-responsive clusters showed significant gene membership overlap with signaling submodules induced (clusters 3, 5, 6, 13, and 24) or repressed (cluster 1) by ABA. GO category enrichment of these ABA-associated clusters identified only one of them as being obvious targets of this pathway (cluster 6, response to ABA stimulus, P value < 1E-8). Other clusters, such as cluster 13 (helicase activity, P value < 1E-6, ATP-dependent chromatin remodeling, P value < 1E-4) and cluster 5 (Cys-type endopeptidase inhibitor activity, P value < 1E-3), were enriched for biological activities that are less well characterized in terms of their association with the salt stress response.

Clusters that were associated with ABA-inducible submodules contained genes that were also activated by salt treatment, suggesting that ABA may directly regulate their transcriptional induction. Three of the six clusters (6, 13, and 24) showed salt-induced expression in all tissue layers, which suggested that ABA signaling is induced in most tissue layers of the root. Importantly, however, clusters 3 and 5 showed highly cell type–specific transcriptional responses, which indicated that ABA signaling was also able to regulate very spatially resolved downstream pathways.

We compared the temporal profiles of the hormone response submodules with the salt response clusters to generate hypotheses about the regulatory mechanisms at work. For example, the salt-regulated clusters that showed peak expression at 1 h (Figure 3A, clusters 6, 13, and 24) were associated with ABA submodules showing rapid activation by hormone treatment at 1 h, whereas salt-regulated clusters showing peak expression at 3 h (clusters 3 and 5) were associated with ABA submodules induced at 3 h. These data suggested that the timing of transcriptional induction in response to NaCl may simply be a function of temporal progression through the ABA response.

To understand what essential roles ABA signaling played in these transcriptional responses, we examined the effect of a mutant in the ABA biosynthetic pathway on salt regulated expression.
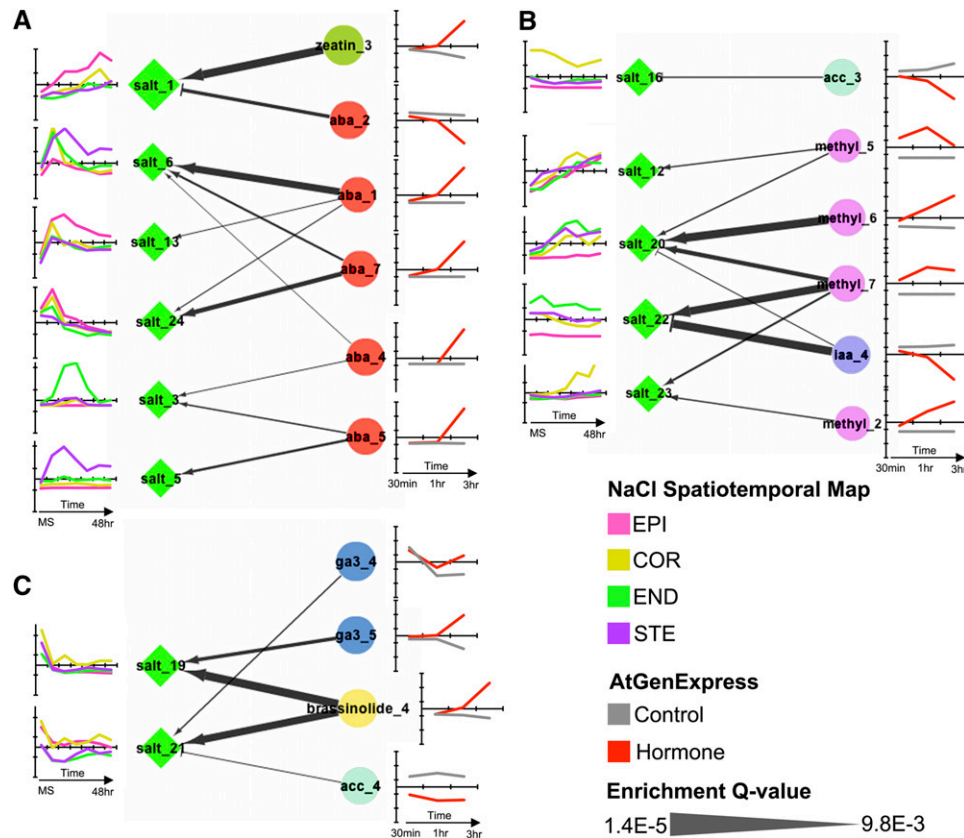
Figure 3. Analysis of the Hormone Secondary Signaling Network Regulating Salt-Dependent Transcriptional Programs.

(A) to **(C)** The secondary signaling network shows the association of hormone response submodules and salt-responsive clusters. The thickness of the edge linking various nodes represents the statistical confidence of such association. The type of arrowhead indicates the predicted regulatory nature of the hormonal interaction as either activating (pointed arrow head) or repressive (blocking arrow head), which is based on the response of genes in the submodule to hormone treatment. The average expression pattern of genes in each submodule (right side) and each salt-responsive cluster (left side) are shown. Treatment conditions for hormones are as follows: aba, 10 μM ABA; zeatin, 1 μM zeatin; ga3, 1 μM GA-3; brassinolide, 10 nM brassinolide; acc, 10 μM 1-aminocyclopropane-1-carboxylic acid; iaa, 1 μM indole-3-acetic acid; methyl, 10 μM methyl jasmonate.
(A) The ABA signaling network is composed of the largest number of salt-regulated clusters.
(B) The JA signaling network is predicted to modulate late-regulated transcriptional programs.
(C) The GA/BR signaling network is predicted to regulate the expression of clusters associated with growth.

The *ABA DEFICIENT 2-sail* (*aba2-sail*) allele does not produce detectable full-length transcripts and similar alleles have been shown to have severe reductions in ABA content (see Supplemental Figure 8 online) (González-Guzmán et al., 2002). We found that many genes that peaked at 1 or 3 h after salt treatment were inhibited in their expression in *aba2-sail* mutants (Figure 4), which was consistent with our predictions.

Our secondary signaling network also predicted that ABA was an important repressor of certain transcriptional programs. Salt-regulated cluster 1, which is induced late in the time course, is associated with an ABA-repressed submodule (Figure 3A). Based on the temporal expression pattern of ABA-induced genes, we predicted that ABA levels were highest early in the time course; thus, we hypothesized that ABA might prevent the early activation of genes in cluster 1. While our quantitative PCR analysis of wild-type roots was not able to reproducibly detect the late salt-mediated activation of these genes, we were able to

observe clear hyperactivated expression in the *aba2-sail* mutant background between 1 and 3 h, as predicted (Figure 4). Together these data showed that ABA signaling was essential for promoting expression of genes early in the salt stress time course and for preventing precocious activation of late expressed genes.

Dynamic Changes Characterize ABA Biosynthesis and Signaling Pathway Components

To determine how the predicted functions of ABA in the salt response corresponded to the actual temporal dynamics of ABA biosynthesis and degradation, we quantified the levels of ABA and its degradation products in whole roots treated with salt stress using liquid chromatography–mass spectrometry (Figure 5A). We observed a dramatic increase in ABA that peaked between 3 and 6 h of salt treatment (Figure 5A). Importantly, ABA levels at 24 h of salt treatment were also elevated compared
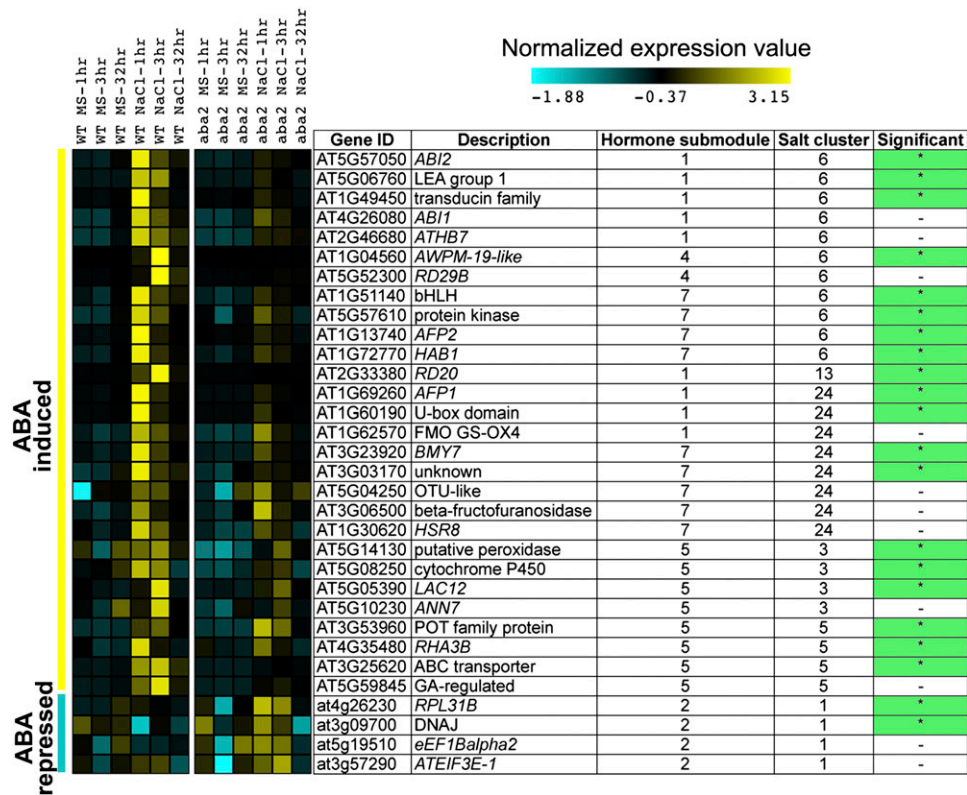
Figure 4. ABA Biosynthesis Regulates Early Activation and Repression of Transcriptional Programs during Salt Stress.

A heat map showing the normalized expression of genes in the Col-0 or *aba2-sail* genetic backgrounds after transfer to standard or salt stress conditions for 1, 3, or 32 h. The hormone submodule association and salt cluster IDs are shown in the table. Expression measured using qRT-PCR from RNA isolated from whole roots. A two-way ANOVA was used to identify genes showing significant genotype by environment effects (marked in green, P value < 0.05).

with standard conditions, but to a lesser extent. The timing of peak ABA levels correlated with that of the ABA responsive reporter *ProRESPONSIVE TO ABA 18:GFP* (*ProRAB18:GFP*) (Kim et al., 2011), which was expressed in the early maturation zone between 4 and 8 h of salt treatment and was then repressed (Figures 5B and 5C; see Supplemental Figure 9 online). The initial degradation product of ABA, phaseolic acid, showed a similar trend of accumulation, while dihydrophaseic acid, which is the final catabolic product of ABA, rose thereafter, and peaked by 24 h (Figure 5A) (Finkelstein and Rock, 2002). These data indicated that ABA biosynthesis was dynamically regulated with peak levels associated with the early phases of the salt stress response, consistent with our prediction.

Production of ABA uses products of the carotenoid biosynthesis pathway with ABA DEFICIENT1 (ABA1) (zeaxanthin epoxidase) acting upstream of NCEDs (for 9-*cis*-epoxycarotenoid dioxygenase), which perform the rate-limiting step (Figure 5D) (Finkelstein and Rock, 2002; Tan et al., 2003). ABA2 and ABA3 act at later steps. Based on our spatio-temporal map, *ABA1* and *NCED3* expression peaked between 1 and 3 h after salt treatment with *NCED3* being the most strongly regulated gene in the pathway (Figure 5D). Thus, consistent with the rate-limiting activity of NCEDs in ABA biosynthesis and the observed timing of

peak ABA levels, *NCED3* is likely the primary determinant regulating the rise in ABA levels. This prediction is also in agreement with previous studies examining the role of this gene in drought response (Iuchi et al., 2001).

We were also curious how ABA degradation might be transcriptionally regulated. *CYP707A1* was the most strongly expressed member of the subfamily of cytochrome P450s directing conversion of ABA to phaseolic acid in the root and showed a similar temporal trend as *NCED3*, indicating that synthesis and degradation pathways are tightly coregulated (Figure 5D) (Kushiro et al., 2004; Saito et al., 2004). Based on the AtGenExpress consortium data (Kilian et al., 2007), *CYP707A1* was induced by ABA treatment (see Supplemental Data Set 6 online), thus revealing a potential negative feedback loop that degrades ABA soon after it is synthesized. *ABA1*, *ABA2*, *NCED3*, and *CYP707A1* each showed different spatial patterns of expression, indicating that ABA metabolism may be distributed across multiple tissue layers.

The ability of cells to transduce an ABA signal requires the presence of hormone receptors; thus, we analyzed the spatio-temporal dynamics of expression for the *PYRABACTIN RESISTANCE/PYRABACTIN RESISTANCE-LIKE/REGULATORY COMPONENT OF ABA RECEPTOR* (*PYR/PYL/RCAR*) family of
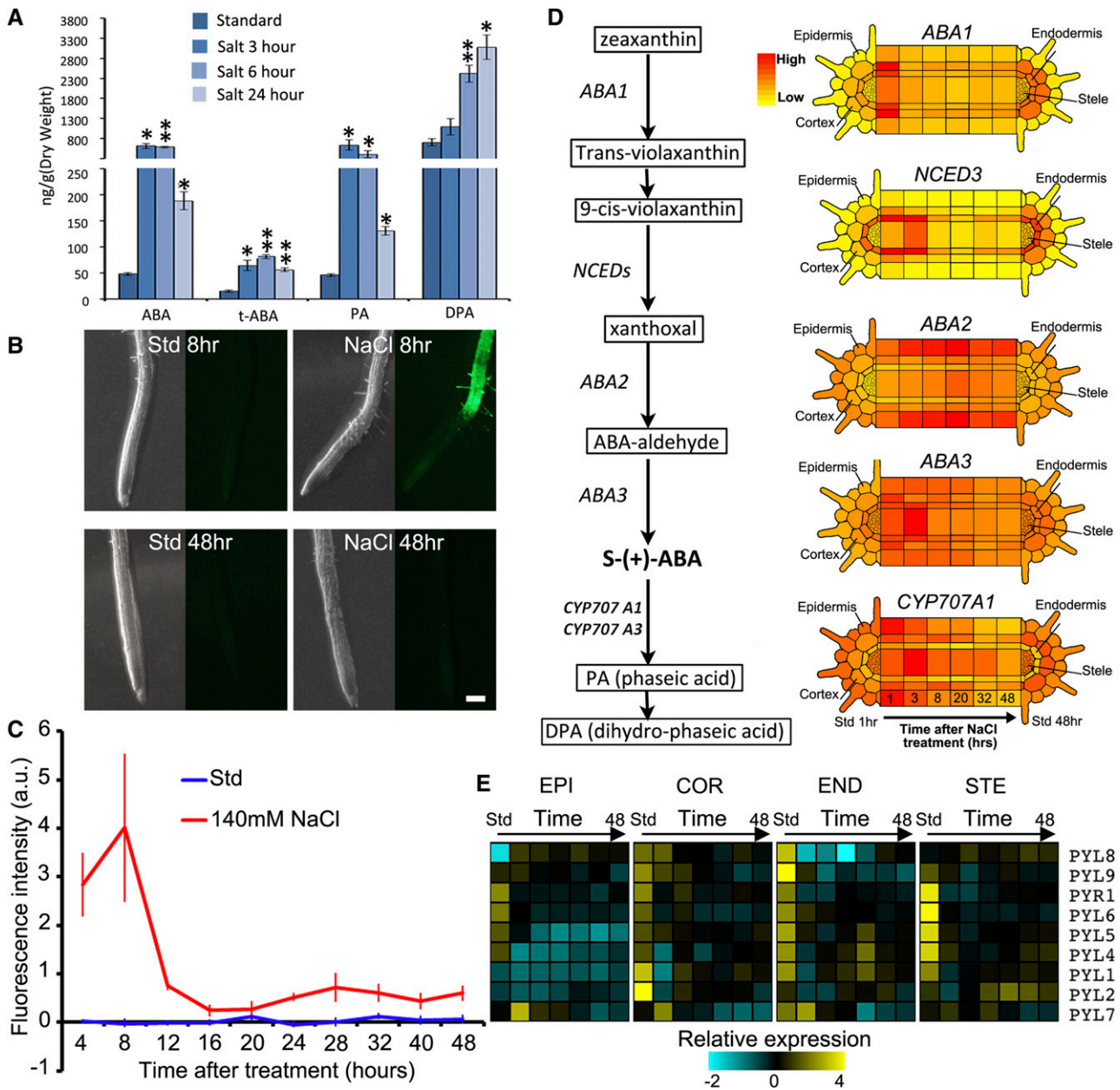
Figure 5. ABA Biosynthesis and Signaling Are Regulated at the Spatio-Temporal Level during Salt Stress.

(A) Quantitation of ABA and ABA metabolites in whole roots isolated after transfer to standard or salt stress conditions. t-ABA, *trans*-isomer of ABA; PA, phaseic acid; DPA, dihydro-phaseic Acid. Three biological replicates were performed.
(B) Fluorescence images of the *ProRAB18:GFP* reporter line transferred to standard or salt stress medium for 8 or 48 h. Note, reporter expression peaks after 8 h of treatment in the early maturation zone. Bar = 100 μm.
(C) Quantitation of GFP fluorescence in the early maturation zone of roots expressing the *ProRAB18:GFP* reporter (*n* = 5).
(D) The ABA biosynthetic pathway is illustrated, and eFP representations show the expression of associated genes significantly differentially expressed during salt stress.
(E) Heat map showing the normalized spatiotemporal expression patterns for members of the *PYL/RCAR* gene family. *PYL3* is not shown due to low expression levels in the root.
Error is SE.

genes encoding ABA receptors to determine if this would predict the pattern of ABA signaling (Ma et al., 2009; Park et al., 2009). The expression of *PYR/PYL/RCAR* genes was highest under standard conditions with several members of the family expressed in each cell layer (Figure 5E). Interestingly, expression of nearly all gene members was immediately repressed during salt stress and recovered partly between 8 to 20 h after treatment. These data suggested that all cell layers are likely able to perceive ABA under standard conditions and immediately after salt treatment, but this responsiveness may be rapidly repressed as protein turnover clears the receptors from the cells. Promoter-reporter studies of a subset of *PYL/RCAR*s have shown that exogenous ABA treatment causes significant downregulation of reporter activity (González-Guzman et al., 2012; Antoni et al., 2013). Together, these data suggest that another negative feedback loop is used during ABA-mediated signaling whereby the capacity of cells to signal the presence of ABA is strongly suppressed. One interesting exception to the trend was *PYL7*, which was activated at 1 h after salt treatment, though the expression of this gene also became repressed after 3 h (Figure 5E).

ABA Biosynthesis and Signaling Promote Growth Recovery during the Late Phases of the Salt Response

We next asked what role ABA signaling played in regulating the dynamics of growth during the salt stress time course. Studies in maize have revealed that ABA promotes growth under water stress by suppressing the biosynthesis of ethylene (Spollen et al., 2000). Consistent with these studies, we found that *Arabidopsis* roots transferred to 140 mM NaCl media supplemented with the ABA biosynthesis inhibitor fluridone exhibited reduced growth rates during the recovery phase of the salt response (Figure 6A). Roots displayed a constitutive increase in radial-cell expansion and root hair development, all hallmarks of the late quiescent phase of the salt response or increased ethylene signaling (Figure 6B) (Schaller and Kieber, 2002; Dinneny et al., 2008). The effects of fluridone in this process are likely due to changes in ABA biosynthesis and not off-target effects as we observed similar but weaker effects in the *aba2-sail* mutant (Figure 6C). The ABI3 transcription factor plays a central role in regulating ABA-mediated responses (Giraudat et al., 1992). While the *abscisic acid insensitive3-1* (*abi3-1*) mutant showed a subtle but significant reduction in growth rates at several time points (Figure 6D), overexpression of an HA-tagged version of ABI3 led to a clearly hastened entrance into the recovery phase by 2 h (Figure 6E) (Xi et al., 2010). Together, these data suggested that ABA biosynthesis and signaling promote growth recovery during salt stress.

Intriguingly, the function of ABA in growth recovery was temporally displaced from the time at which ABA levels peaked. To determine whether low levels of ABA biosynthesis, which occurred at late time points, were necessary for growth promotion during the recovery and homeostasis phases, we treated roots with fluridone during specific windows of time during the salt response. These experiments showed that ABA biosynthesis was most critical during the homeostasis and recovery phases to promote growth, while fluridone treatment during the first 8 h of the salt response had little effect on later growth (Figure 6F).

Cell Type–Specific Manipulation of ABA Signaling Highlights the Importance of Specific Tissues in Mediating Transcriptional and Growth Responses to Salt Stress

Several growth-promoting plant hormones have been shown to act through tissue-specific signaling. To determine whether ABA signaling functions by similar principles, we previously developed a strategy involving the misexpression of the *abi1-1* coding sequence to inhibit ABA signaling in specific cell layers (Duan et al., 2013). The *abi1-1* mutant allele encodes a protein that is disrupted in its ability to bind to the ABA coreceptors, PYR/PYL/RCAR, which inhibit the phosphatase activity of the wild-type ABI protein upon ABA perception (Fujii et al., 2009). We used the GAL4-VP16/UAS transactivation system to drive spatially localized expression of a *UAS:abi1-1* transgene in the root and monitored the impact of these changes in ABA signaling on salt-regulated gene expression in root tips using high-throughput qRT-PCR (Figures 7A and 7B). We focused our analysis on transcriptional changes that occurred after 1 h of treatment since this is within the time period where the transcriptional effects of ABA are most prevalent. Genes were selected for qRT-PCR expression analysis that were members of our salt-regulated clusters and associated with ABA submodules. Of the 94 genes assayed, we found that 30 genes showed significant genotype by environment effects (two-way analysis of variance (ANOVA), multiple-testing corrected P value < 0.01). Of the 11 genes that were upregulated, *abi1-1* expression had the greatest impact on the salt stress response when driven by the Q2500 enhancer trap, which drives strong expression in the endodermis and weaker expression in the pericycle of the primary root (Figures 7A and 7B).

Several genes showed an intriguing correlation between their expression pattern based on the spatio-temporal map and the cell layers where ABA signaling was most critical for salt regulation. For example *At5g14130*, which encodes a protein with predicted peroxidase activity, was specifically activated in the endodermis based on our spatio-temporal map and was strongly dependent on ABA signaling in the END/PER tissue layers (Figures 7B and 7C). *SNF1-RELATED KINASE2.6* (*SNRK2.6*), which encodes a kinase necessary for ABA-mediated signal transduction, was activated most strongly by salt in the inner tissue layers of the root (Figure 7D) and was also dependent upon ABA signaling in these same cell layers (Figure 7B).

Salt-mediated transcriptional repression was also affected by *abi1-1* misexpression. We had previously shown that *COBRA*, which encodes a GPI-anchored protein important for cell wall biosynthesis, is downregulated by salt in the outer tissue layers and is important for regulating changes in cell shape that occur in the epidermis and cortex (Dinneny et al., 2008). Here, we found that *COB* expression is particularly affected by ABA signaling in the outer tissue layers under standard conditions along with two other genes encoding proteins likely involved in cell wall biosynthesis (*CELLULOSE SYNTHASE LIKE A9* [At-CSLA9], pectate lyase; Figures 7B and 7E). ABA signaling also appeared to be important for fully repressing expression under salt stress conditions for these three genes.

We also assayed the role of tissue-specific ABA signaling in regulating the expression of genes in salt cluster 1, which we
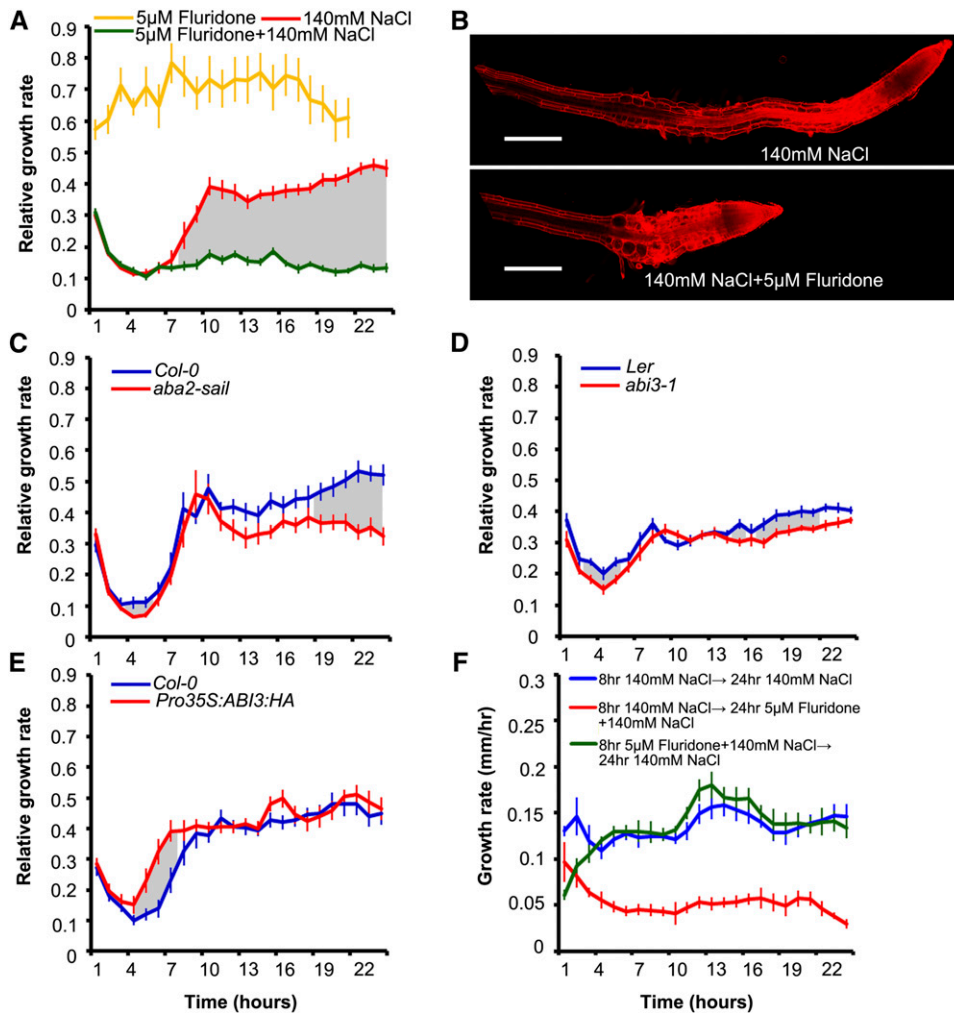
Figure 6. ABA Biosynthesis and Signaling Are Necessary to Promote Full Growth Recovery during Salt Stress.

(A) Effect of fluridone treatment on growth under standard or salt stress conditions. Fluridone treatment strongly inhibited the ability of the root to recovery growth rates after salt treatment. Col-0 standard (n = 8), Col-0 5 μM fluridone (n = 8), Col-0 140 mM NaCl (n = 15), Col-0 5 μM fluridone, and 140 mM NaCl (n = 15).

(B) Confocal images of roots transferred to salt stress conditions (top panel) or salt stress conditions including 5 μM fluridone (bottom panel). Note that the increase in radial cell expansion induced by salt stress had occurred for an extended period of time with fluridone treatment (scale bar is 250 μm).

(C) The *aba2-sail* mutant causes a reduction in growth rates during the homeostasis phase. Col-0 standard (n = 12), Col-0 140 mM NaCl (n = 12), *aba2-sail* standard (n = 8), and *aba2-sail* 140 mM NaCl (n = 16).

(D) The *abi3-1* mutation caused a subtle reduction in growth during the quiescent and homeostasis phases. Landsberg *erecta* standard (n = 8), Landsberg *erecta* 140 mM NaCl (16), *abi3-1* standard (n = 8), and *abi3-1* 140 mM NaCl (n = 16).

(E) The *Pro35S:ABI3:HA* transgenic line hastened growth recovery by several hours. Col-0 standard (n = 8), Col-0 140 mM NaCl (n = 16), *ProABI3:ABI3: HA* standard (n = 8), and *ProABI3:ABI3:HA* 140 mM NaCl (n = 16).

(F) Live imaging analysis of root growth rates after transfer to salt medium supplemented with fluridone at different time points during the salt stress response. Col-0 seedlings were transferred to 140 mM NaCl medium for 8 h then transferred to fresh 140 mM NaCl medium and imaged for 24 h (n = 8), Col-0 seedlings were transferred to 140 mM NaCl medium for 8 h then transferred to 140 mM NaCl medium with 5 μM fluridone and imaged for 24 h (n = 8), and Col-0 seedlings were transferred to 140 mM NaCl medium with 5 μM fluridone for 8 h then transferred to 140 mM NaCl medium for 24 h (n = 8). Growth data are presented as a percentage of difference in growth rate relative to standard conditions except F, which shows growth rate. Error is SE. A two-tailed Student's *t* test was performed for each time point between conditions. Significant differences are shown using gray shading (P value < 0.05).
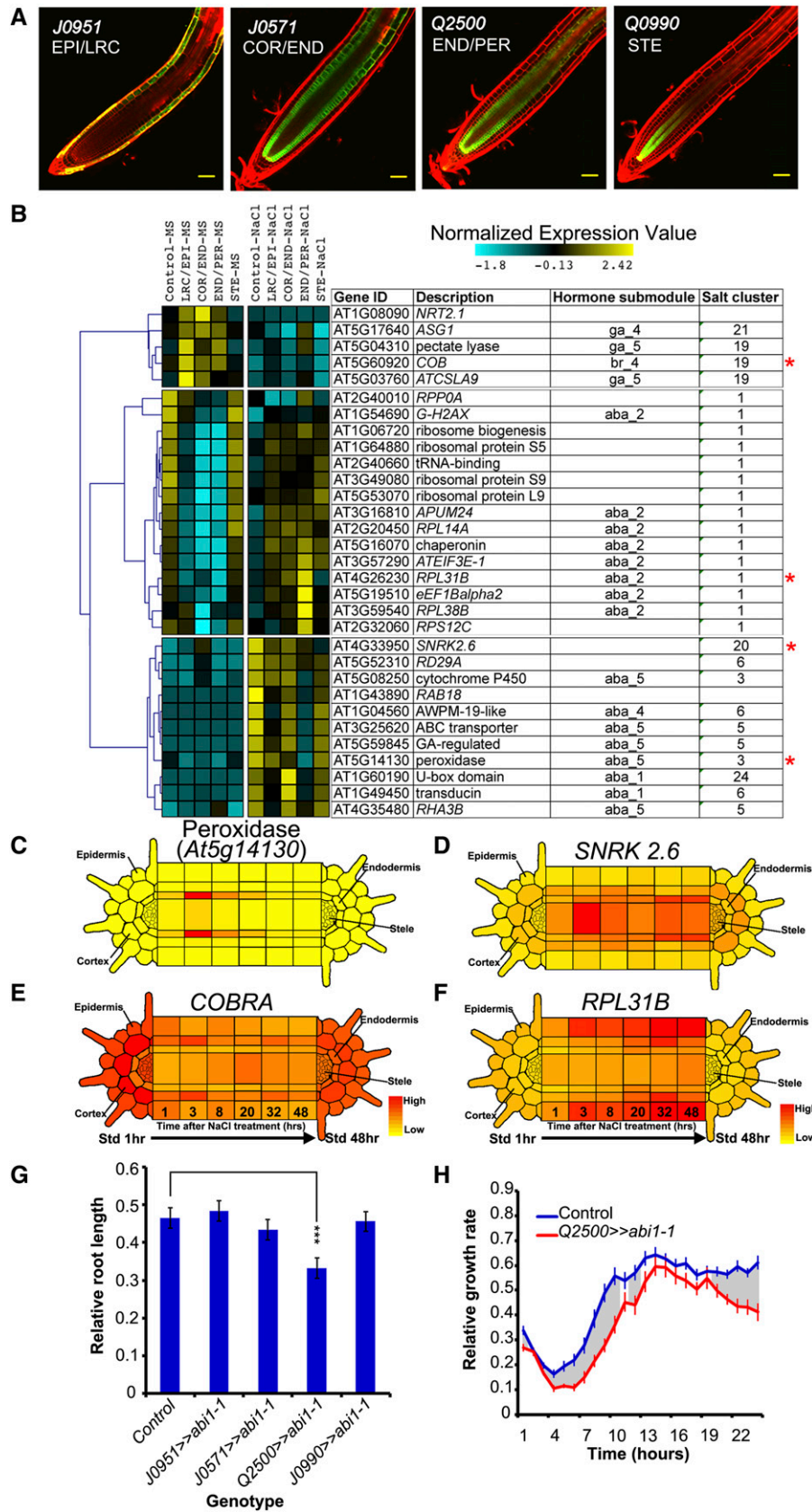
Figure 7. Cell Layer–Specific ABA Signaling Regulates Spatially Localized Transcriptional Changes and Growth.

Panel B table (Normalized Expression Value):

Gene ID	Description	Hormone submodule	Salt cluster	
AT1G08090	NRT2.1			
AT5G17640	ASG1	ga_4	21	
AT5G04310	pectate lyase	ga_5	19	
AT5G60920	COB	br_4	19	*
AT5G03760	ATCSLA9	ga_5	19	
AT2G40010	RPP0A		1	
AT1G54690	G-H2AX	aba_2	1	
AT1G06720	ribosome biogenesis		1	
AT1G64880	ribosomal protein S5		1	
AT2G40660	tRNA-binding		1	
AT3G49080	ribosomal protein S9		1	
AT5G53070	ribosomal protein L9		1	
AT3G16810	APUM24	aba_2	1	
AT2G20450	RPL14A	aba_2	1	
AT5G16070	chaperonin	aba_2	1	
AT3G57290	ATEIF3E-1	aba_2	1	
AT4G26230	RPL31B	aba_2	1	*
AT5G19510	eEF1Balpha2	aba_2	1	
AT3G59540	RPL38B	aba_2	1	
AT2G32060	RPS12C		1	
AT4G33950	SNRK2.6		20	*
AT5G52310	RD29A		6	
AT5G08250	cytochrome P450	aba_5	3	
AT1G43890	RAB18			
AT1G04560	AWPM-19-like	aba_4	6	
AT3G25620	ABC transporter	aba_5	5	
AT5G59845	GA-regulated	aba_5	5	
AT5G14130	peroxidase	aba_5	3	*
AT1G60190	U-box domain	aba_1	24	
AT1G49450	transducin	aba_1	6	
AT4G35480	RHA3B	aba_5	5	

predicted to be a target of ABA-mediated repression early in the time course. Interestingly, we found that several of these genes, including *RIBOSOMAL PROTEIN L31B* (*RPL31B*), showed significant derepression under salt stress conditions when ABA signaling was inhibited in the END/PER layers (Figures 7B and 7F). Unexpectedly, we found that ABA signaling in the LRC/EPI, COR/END, and END/PER was necessary to promote the expression of these genes under standard conditions. These later results are not readily interpretable but suggest complex roles for ABA signaling in regulating protein translation under non-stress conditions.

To determine what function tissue-specific ABA signaling plays in regulating primary root growth, we transferred seedlings of the various transactivation genotypes to standard or salt stress conditions and measured root length after 24 h. Similar to the results of our transcriptional analysis, root growth was most dramatically affected when *abi1-1* expression was driven in the END/PER tissue layers (Figure 7G). Live-imaging analysis revealed that the *Q2500>>abi1-1* transactivation line showed delayed recovery and reduced growth during the homeostasis phase of the salt response (Figure 7H). These data are consistent with ABA signaling being important for promoting growth during the recovery phase and highlight the END/PER cell layers as being particularly important in this regard.

JA Activates Defense Pathways during Salt Stress and Inhibits Growth Recovery

Based on our bioinformatic analysis, JA signaling was predicted to promote the expression of genes in four different salt-regulated clusters (Figure 3B). Clusters 12, 20, and 23 were stably upregulated after 3 h of salt response. Cluster 22 was the exception and was repressed by salt; however, this cluster was also strongly associated with an indole-3-acetic acid–responsive submodule that was predicted to repress the expression of this

cluster, and this may modify the effects of JA signaling on gene expression. All three clusters tended to be induced by salt stress in the inner tissue layers of the root, indicating some spatial regulation of this signaling pathway. Indeed, based on the spatio-temporal map, *JASMONATE INSENSITIVE3*, which functions as a repressor of the JA pathway, showed EPI-enriched expression throughout the salt response (see Supplemental Figure 10A online).

Clusters 20 and 23 were both enriched for genes associated with biotic defense (cluster 20, callose deposition in cell wall during defense response, P value < 1E-9, glucosinolate biosynthetic process P value < 1E-7; cluster 23, response to biotic stimulus, P value < 1E-6). These biological processes are not obviously related to the regulation of growth; however, previous studies have shown that JA can also negatively regulate both meristem size and cell elongation (Chen et al., 2011). Thus, we asked whether loss of JA signaling affected the growth of the root during salt stress using the JA resistant mutant allele *jai3-1*, which encodes a negative regulator of the pathway that is resistant to JA-mediated protein degradation (Chini et al., 2007). Under salt stress, *jai3-1* mutant roots entered the recovery phase 1 h earlier than the wild type and showed an increased growth rate during the first 7 h of the homeostasis phase (Figure 8A). Both results are consistent with a role for JA in growth repression during these later phases of the salt response.

Dynamic Repression of GA and BR Signaling during Salt Stress Regulates Growth Quiescence

We next turned our attention to hormone pathways known to promote growth in the root. GA submodules were associated with salt-regulated clusters (clusters 19 and 21), which showed early transcriptional repression and late recovery during the stress response (Figure 3C). Both clusters showed peak expression in the COR and/or EPI tissue layers, suggesting that

---

Figure 7. (continued).

(A) Expression of the *UAS:erGFP* reporter from the four different *GAL4-VP16* enhancer-trap lines used in this study. *J0951* drives expression in the epidermis (EPI) and lateral root cap (LRC), *J0571* expresses in the cortex (COR) and endodermis (END), *Q2500* expresses in the END and pericycle (PER) cell layers, and *Q0990* expresses in the stele (STE). Bar = 20 μm.

(B) Heat map showing the normalized expression of salt responsive genes in the control genotype and different transactivation lines expressing the *abi1-1* mutant protein in select tissue layers. Expression measured using qRT-PCR from RNA isolated from whole roots. Asterisks mark genes described in more detail in text and in **(C)** to **(F)**.

(C) to **(F)** eFP diagrams show expression of a selection of genes analyzed in **(B)**.

(C) A peroxidase (At5g14130) shows enriched expression in the endodermis between 3 and 8 h after salt treatment, which is strongly disrupted when ABA signaling is disrupted in the END/PER layers.

(D) *SNRK2.6* (At4g33950) is activated in the stele at 3 h and is strongly dependent on ABA signaling in the STE tissue layers.

(E) *COBRA* (At5g60920) is dynamically repressed in the cortex and becomes hyperactivated under standard conditions if ABA signaling is repressed in several different tissue layers.

(F) *RPL31B* (At4g26230) shows increased expression the epidermis late in the time course and becomes hyperactivated under salt stress conditions when ABA signaling is suppressed in the END/PER cell layers.

(G) Relative root length of various transactivation lines after transfer to salt stress conditions. Relative root length calculated as the ratio between the length under salt stress conditions and that under standard conditions after growth for 2 d (*n* is greater than 10 for each genotype and condition).

(H) Live imaging analysis of the *Q2500>>abi1-1* transactivation line and associated control under salt stress conditions. Control genotype standard (*n* = 16), control genotype 140 mM NaCl (*n* = 24), *Q2500>>abi1-1* standard (*n* = 16), and *Q2500>>abi1-1* 140 mM NaCl (*n* = 24).

Growth data are presented as a percentage of difference in growth rate relative to standard conditions. Error is SE. A two-tailed Student's *t* test was performed for each time point between conditions. Significant differences are shown using gray shading (P value < 0.05).

GA levels may decline in these regions of the root. While we were not able to reproducibly detect the various forms of GA in our study, other studies have shown that GA levels fall upon salt treatment and the RGA1 protein, which is a repressor of GA-mediated growth, is stabilized (Achard et al., 2006). The *ProRGA1:GFP:RGA1* reporter can be used to track GA signaling, as GA perception leads to the degradation of the GFP:RGA1 protein. Indeed, we observed that GFP:RGA1 fluorescence intensity increased between 5 to 8 h after salt treatment and diminished by 48 h (Figures 8B and 8C), which correlated well with the predicted dynamics of GA signaling.

The reduction in GFP:RGA1 fluorescence late in the salt response suggested that GA signaling may partially recover at these times and play a positive role in the reactivation of growth. We tested this hypothesis by performing live imaging of salt-treated roots supplemented with paclobutrazol (PAC), a GA biosynthesis inhibitor (Rademacher, 2000). In contrast with the control salt treatment where roots recovered growth between 7 to 10 h after treatment, PAC treated roots were strongly inhibited

in their recovery (Figure 8D). To test the effects of increased GA signaling on the salt stress response, we performed live imaging analysis of the *della quadruple* mutant (Tyler et al., 2004). The effects of this mutant were subtle but did reveal increased growth at later time points (Figure 8E). Together, these data showed that GA biosynthesis and signaling are likely necessary during the late phases of the salt response to promote recovery and suggested that dynamic changes in the biosynthesis of this hormone are critical for determining the temporal pattern of growth regulation during salt stress.

BR signaling is predicted to promote the expression of genes in the same salt-responsive clusters as GA (Figure 3C). Thus, similar to GA, we predicted that BR signaling was dynamically suppressed during salt stress and contributed to the temporary reduction in growth rate observed during these time points. BR perception leads to dephosphorylation of the BRASSINOZOLE RESISTANT1 (BZR1) transcription factor, nuclear localization of the protein, and regulation of downstream transcriptional targets such as *DWARF4* (*DWF4*) (Wang et al., 2002; He et al., 2005).
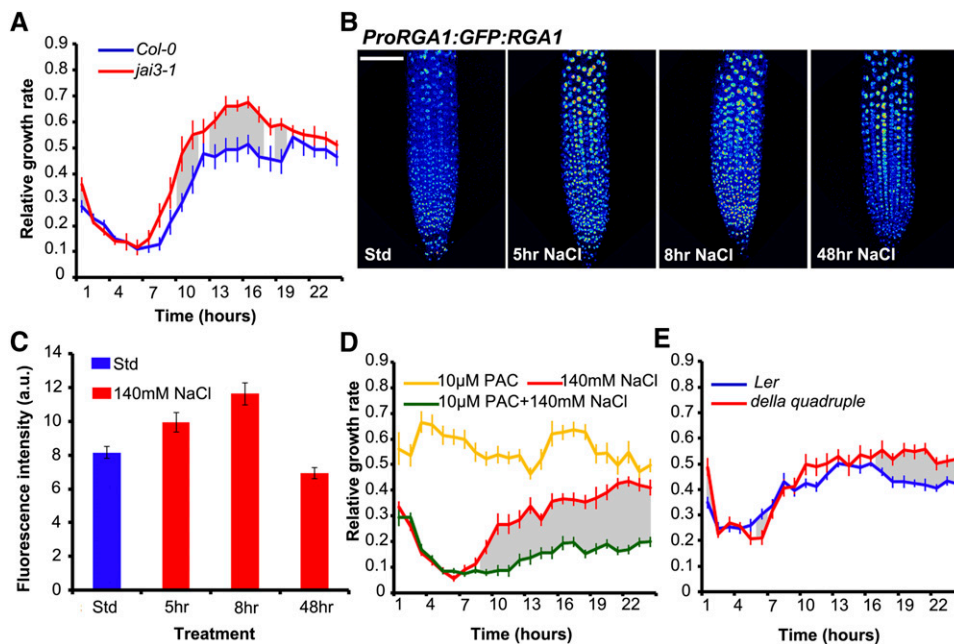

Figure 8. JA Suppressed Growth Recovery and GA Signaling Was Dynamically Regulated during Salt Stress.

(A) Live imaging analysis of salt response in the primary root in Col-0 and *jai3-1* mutants. Col-0 standard (*n* = 8), Col-0 140 mM NaCl (*n* = 14), *jai3-1* standard (*n* = 8), and *jai3-1* 140 mM NaCl (*n* = 16).

(B) Confocal images showing the maximum intensity projection of fluorescence from a root tip expressing the *ProRGA1:GFP:RGA1* reporter. Fluorescence is shown in roots after transfer to standard or salt stress medium for various lengths of time. Fluorescence signal shown using the Rainbow LUT setting in ImageJ to more clearly show differences in intensity (blue, low; red, high). Bar = 100 μm.

(C) Quantitation of GFP intensity at different time points after salt treatment in *ProRGA1:GFP:RGA1* expressing roots (*n* is greater than five for each condition).

(D) Effect of PAC treatment on growth under standard or salt stress conditions. PAC treatment strongly inhibited the ability of the root to recover growth rates after salt treatment. Col-0 standard (*n* = 8), Col-0 140 mM NaCl (*n* = 15), Col-0 10 μM PAC (*n* = 8), and Col-0 140 mM NaCl with 10 μM PAC (*n* = 15).

(E) Effect of the *della quadruple* mutant on the salt response. Significant differences in growth rates were only observed during the recovery phase. Landsberg *erecta* standard (*n* = 8), Landsberg *erecta* 140 mM NaCl (*n* = 16), *della quadruple* standard (*n* = 8), and *della quadruple* 140 mM NaCl (*n* = 16). Growth data are presented as a percentage of difference in growth rate relative to standard conditions. Error is SE. A two-tailed Student's *t* test was performed for each time point between conditions. Significant differences are shown using gray shading (P value < 0.05).
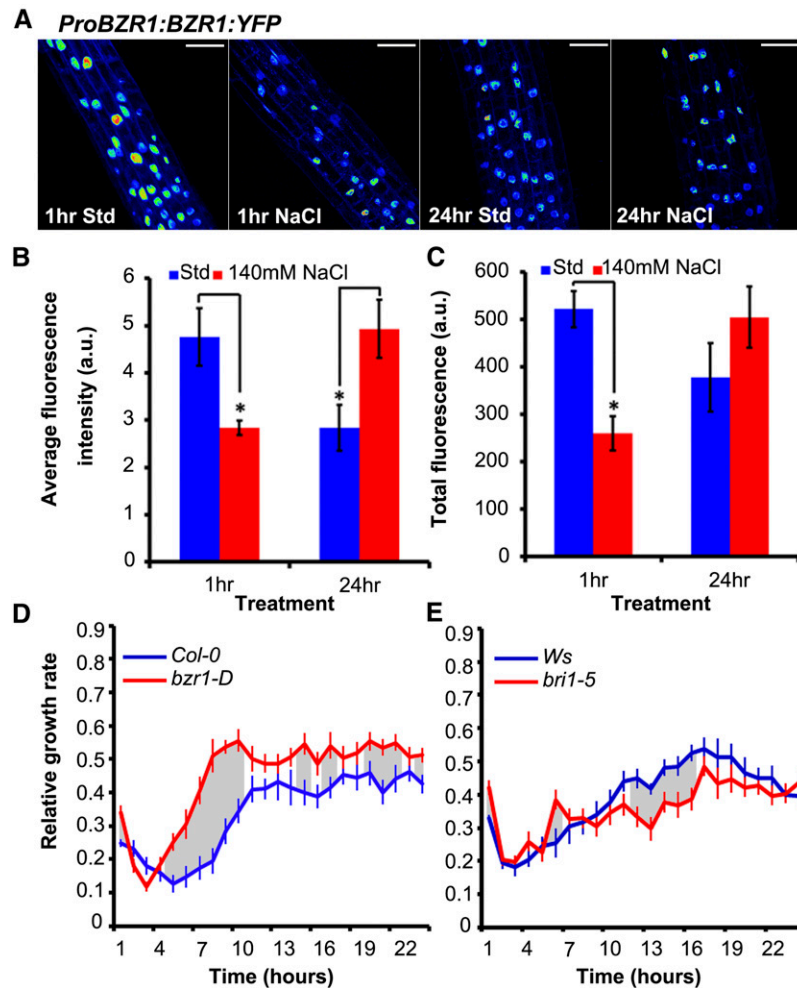
Figure 9. BR Signaling Is Dynamically Suppressed during Salt Stress and Is Sufficient to Promote Early Growth Recovery.

(A) Maximum projection of fluorescence from confocal images of roots expressing the *ProBZR1:BZR1:YFP* reporter. Fluorescence signal shown using the Rainbow LUT setting in ImageJ to more clearly show differences in intensity (blue, low; red, high). Bar = 50 μm.

(B) Quantification of average fluorescence of nuclei in the epidermal tissue layer from the elongation zone. Note that a significant decrease in average fluorescence was observed at 1 h of treatment. Fluorescence recovered under salt stress conditions but dropped under standard conditions. These differences may be due to changes in the size of the nucleus ($n = 9$).

(C) Total fluorescence quantified in nuclei of the epidermal tissue layer in the elongation zone. Note that measuring total fluorescence corrected for changes in nuclear volume and showed that significant differences in BZR1:YFP accumulation are only observed at 1 h after treatment ($n = 9$).

(D) The *bzr1-D* mutation had a significant effect on the growth profile of the root under salt stress conditions, where the time to recovery was hastened by ~5 h. Growth rates were also higher during the recovery phase. Col-0 standard ($n = 8$), Col-0 140 mM NaCl ($n = 16$), *bzr1-D* standard ($n = 8$), and *bzr1-D* 140 mM NaCl ($n = 16$).

(E) The *bri1-5* mutant is weakly insensitive to BR treatment and showed a modest reduction in growth recovery compared with the Wassilewskija ecotype control. Wassilewskija standard ($n = 8$), Wassilewskija 140 mM NaCl ($n = 16$), *bri1-5* standard ($n = 8$), and *bri1-5* 140 mM NaCl ($n = 16$).

Growth data are presented as a percentage of difference in growth rate relative to standard conditions. Error is SE. A two-tailed Student's *t* test was performed for each time point between conditions. Significant differences are shown using gray shading (P value < 0.05).

We used the *ProBZR1:BZR1:YFP* (for yellow fluorescent protein) reporter line to profile changes in BR signaling over time during salt stress. Fluorescence intensity in nuclei of cells in the elongation zone of the root showed a significant decrease after 1 h of treatment (Figures 9A and 9B). After 24 h, the average fluorescence intensity recovered. Quantification of the YFP signal in nuclei was difficult to interpret under salt stress as the size of the

nucleus was affected by the treatment. Thus, total fluorescence was also quantified per nucleus and clearly showed that the amount of BZR1:YFP in the nucleus was not significantly different at 24 h of growth on standard or salt stress media (Figure 9C). These results suggested that BR signaling was temporarily suppressed during the early phase of the salt response and recovered later. These data are also consistent with the dynamic

expression pattern of *DWF4*, which is directly repressed by BZR1 (He et al., 2005); *DWF4* expression increased in the STE and peaked at 8 h of salt treatment but then fell back to normal levels between 20 to 32 h (see Supplemental Figure 10B online). Consistent with the hypothesis that genes in clusters 19 and 21 are targets of BR signaling during salt stress, we found significant enrichment of BZR1 targets in both gene sets (P value < 6E-8 and 0.03, respectively; see Supplemental Data Set 7 online) (Oh et al., 2012).

To test whether recovery of BR signaling was important for promoting growth during salt stress, we examined the response of the *bzr1-D* mutant, which causes constitutive activation of many BR-dependent processes (Wang et al., 2002). Interestingly, *brz1-D* mutant roots showed a substantially reduced quiescent phase and recovered growth 5 h earlier than the wild type (Figure 9D). In addition, growth rates during the homeostasis phase were also higher. To test whether BR signaling was also necessary for growth recovery, we examined the *brassinosteroid insensitive1-5* (*bri1-5*) mutant, which mildly impairs BR signaling (Noguchi et al., 1999). As expected, we detected a subtle yet significant decrease in recovery phase growth, consistent with the proposed function of BR in promoting growth recovery during salt stress (Figure 9E).

DISCUSSION

We describe here a cell-type resolution analysis of the full temporal landscape of an environmental response in plants from the initial moments of perception to the long-term adjustments leading to transcriptional and growth rate homeostasis. By analyzing both growth and transcriptional regulation at high-temporal resolution and defining transitions in biological functions using our multidimensional microarray data set, we were able to parse out several critical regulatory pathways important for the salt response (Figure 10). We defined the hormonal signals predicted to have the largest role in transcriptional regulation, identified their target pathways and cell types, determined their time of action, and placed this regulation in the developmental context of dynamic root growth regulation. We found that dynamic changes in root growth are not simply a consequence of the inability of the cells to expand but instead are regulated processes orchestrated by hormonal growth repressors and activators that act during discrete phases to hasten or delay the time at which root growth resumes. We speculate that the transition from quiescence to growth recovery may be regulated by many separate physiological pathways acting through different hormones to precisely advance the root through the stress response time course at the appropriate pace.

Hormonal Regulation of Root Growth during Salt Stress: A Model

In work presented here as well as another study we recently published (Duan et al., 2013), we show that ABA signaling acts through internal tissue layers to regulate growth. In the lateral root, ABA signaling acts to suppress growth for an extended length of time, with growth recovery occurring after days of salt
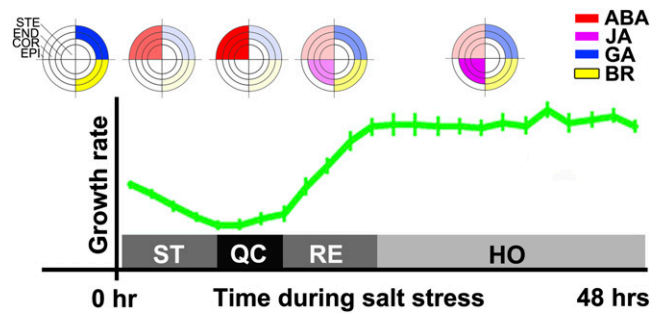

Figure 10. Model for Spatio-Temporal Dynamics in Hormone Signaling and Growth Regulation during the Salt Stress Response.

Diagram shows the inferred timing and spatial pattern of activity for ABA, JA, GA, and BR signaling during the salt stress response time course. ABA levels peak during the ST and QU phases of the salt response, but lower levels present during the RE and HO phases promote growth recovery. Based on experiments using tissue-specific suppression of ABA signaling, the inferred site of ABA in growth regulation is the END/PER tissue layers; however, regulation of gene transcription appears to occur through signaling in all tissue layers. JA levels are predicted to rise during the RE and HO phases, which are when the *jai3-1* mutant has an effect on growth rates and when JA-associated transcriptional programs are induced during the salt response. GA and BR signaling is coregulated with peak levels occurring under nonstress conditions. Based on the expression pattern of GA and BR-associated transcriptional targets and dynamic changes in fluorescent-based reporters of pathway activity, we infer that GA and BR signaling recovers during the RE and HO phases of the salt stress response. Reestablishment of pathway activity is necessary to promote growth recovery.

treatment. At 100 mM NaCl, the primary root does not strongly activate ABA signaling, and we observed that disruption of ABA signaling largely has lateral root-specific effects on growth. Here, we showed that at 140 mM NaCl, ABA signaling was briefly activated in the primary root with peak ABA levels correlating with growth quiescence. Thus, both the primary and lateral roots can activate ABA signaling, but at different threshold concentrations of salt and for very different lengths of time.

Interestingly, while ABA signaling in the lateral root has clear functions in suppressing growth, in the primary root, our data suggest a role in promoting growth. ABA, like many other hormones, has the property that low levels of the hormone promote growth while high levels inhibit growth (Finkelstein and Rock, 2002). In this regard, it is intriguing that the phase of the salt response where ABA biosynthesis is most important for promoting growth is during the recovery and homeostasis phases where we have measured much smaller differences in ABA accumulation compared with control conditions. Our proposed role for ABA in promoting long-term growth recovery during salt stress is similar to that proposed in maize where it has been shown that under water stress, low levels of ABA (~1 μM) promote growth of the primary root through the suppression of ethylene signaling (Spollen et al., 2000).

Our work also identifies important roles for other plant hormones in the salt stress response and places these pathways in a temporal context. Hyperactivation of BR transcriptional regulation using the *bzr-1D* mutant indicates that the timing of

growth recovery during salt stress can be dramatically hastened by as much as 5 h. These data, together with the observations we made using the BZR1-YFP reporter, indicate that a critical outcome of salt stress signaling is the temporary suppression of the BR pathway. Importantly, growth is still strongly repressed for several hours even in *bzr1-D* mutants, which indicates that some component of growth regulation may occur independent of BR hormone regulation. The immediate suppression of growth that occurs with 140 mM NaCl treatment may be a consequence of the physical impediment to cell elongation that is expected to occur after a dramatic change in the osmotic environment of the root.

Our work shows that dynamic hormonal signaling is necessary to properly time the recovery of growth. These events likely require tight coordination with the regulation of other biological processes important for long-term acclimation to a saline environment. Importantly, our work also shows that no single hormonal pathway determines the complete temporal architecture of the salt stress response. It will be critical for future studies to understand the mechanisms that regulate the rate of hormone biosynthesis and catabolism and how these pathways ultimately regulate the growth of the root through cell type–specific signaling. Furthermore, while our secondary signaling network has identified little transcriptional evidence of crosstalk between the hormonal pathways, posttranscriptional crosstalk mechanisms and nonhormonal signaling pathways, such as calcium ions and reactive oxygen species, are likely to be important mechanisms for signal integration.

METHODS

Plant Materials and Growth Conditions

All *Arabidopsis thaliana* GFP reporter lines used for FACS were previously described and are in the Col-0 background (Dinneny et al., 2008). The *aba2-sail* (Duan et al., 2013), *jai3-1* (Chini et al., 2007), and *bzr1-D* mutant alleles (Wang et al., 2002) and the *UAS:abi1-1* (Duan et al., 2013) and *ProRAB18:GFP* (Kim et al., 2011) transgenes are in the Col-0 background. The *della quadruple* mutant allele (Tyler et al., 2004) and the *ProRGA:GFP*: *RGA* (Achard et al., 2006) transgenes are in the Landsberg *erecta* background. The *bri1-5* mutant allele is in the Wassilewskija background (Noguchi et al., 1999). Seed sterilization and growth conditions were as previously described (Duan et al., 2013).

Live-Imaging and Data Analysis

Seedlings were grown and imaged using a custom macroscopic imaging system as previously described (Duan et al., 2013). Growth rates were quantified using a semiautomated image analysis algorithm written as a macro for ImageJ (Abramoff et al., 2004), which is available through our lab's website (http://dinnenylab.dpb.carnegiescience.edu). In brief, the macro requires a stack of time-lapse images to be imported into ImageJ. The macro processes the image stack to enhance the contrast of edges. The user then draws a line in the last frame of the series along the midline of the root from the tip to the base. The algorithm uses the midline as a landmark to aid in identifying the position of the root tip in each frame and translates this position back onto the midline. A table is generated listing the distance between root tip positions between subsequent frames of the time-lapse series. Growth measurements made during 1 h were summed together. To calculate relative growth rate, the average growth rate under control conditions was determined and used to normalize growth under treatment conditions.

Sample Preparation, RNA Isolation, Microarray Hybridization, and Data Analysis: Agilent Array

Seeds were sterilized and stratified at 4°C for 2 d in water. After cold treatment, seeds were sown on nylon mesh over standard medium and grown vertically under long-day conditions for 5 d. Seedlings were transferred to standard medium or medium supplemented with 140 mM NaCl and whole roots were harvested after different lengths of time after transfer. The timing of seed sterilization and sowing was staggered so that the length of time a seed spent at each step was the same. All tissue samples were harvested on the same day within a 2-h time window to ensure minimal influence from circadian regulation on gene expression. Two biological replicates were generated for each sample type.

RNA was extracted using the RNAeasy Miniprep kit (Qiagen) and Cy3-labeled probes synthesized using the Agilent RNA amplification and labeling kit. Probes were hybridized to a 4X44k Agilent Gene Expression Microarray (V4: 021169). Probe hybridization was performed at the Biopolis Shared Facilities, Agency of Science and Technology Research, Singapore according to Agilent's recommended protocol.

All data analyses were performed using the R software package (http://www.r-project.org) and packages provided through Bioconductor (http://www.bioconductor.org). Pairwise comparisons were performed between control and salt stress samples using LIMMA (Smyth, 2005). The Benjamini and Hochberg method was used to calculate false discovery rates. A multiple testing corrected P value threshold of 0.001 was used along with a twofold change cutoff to select differentially expressed genes. GO category enrichment was performed using the ChipEnrich JAVA application (Brady et al., 2007).

Protoplasting of Roots and Isolation of GFP-Enriched Cell Populations by FACS

Seedlings were grown as described above and treatments followed the schedule outlined in Supplemental Table 1 online. Protoplasting of root cells was performed as previously described (Birnbaum et al., 2005). GFP positive cells were sorted using BD FACs Vantage SE into RPE lysis buffer (Qiagen) at the Cell Cytometry Core Facility, NUMI, located at the National University of Singapore, Singapore. The enrichment of GFP-expressing protoplasts in the total population of FACS isolated cells was determined by collecting cells into PBS buffer and counting using a hemocytometer.

RNA Isolation, Microarray Hybridization, and Data Analysis: Affymetrix ATH1 Arrays

Total RNA from 50,000 FACS isolated cells was extracted using the RNAeasy Micro Kit (Qiagen). The yield and quality of total RNA was analyzed using a Nanodrop spectrophotometer and Pico RNA chips on a Bioanalyzer (Agilent Technologies). One hundred nanograms of total RNA was labeled using the GeneChip 3′ IVT Express labeling kit (Affymetrix) and hybridized to ATH1 gene chips following the manufacturer's instructions (Affymetrix). Arrays were washed using a GeneChip Fluidics Station 450 and GeneChip hybridization, wash, and stain kit (Affymetrix) before data acquisition on a GeneChip scanner (Affymetrix). Bioanalyzer analysis and Affymetrix hybridization, washing, and scanning were performed in the microarray facilities located at the Biopolis Shared Facilities, Agency of Science and Technology Research, Singapore. Three biological replicates were performed per sample type.

All data analyses were performed using the R software package (http://www.r-project.org) and packages provided through Bioconductor (http://www.bioconductor.org). GCRMA was used for global normalization

(Irizarry et al., 2006). Data quality was examined using the signal distribution of Affymetrix built-in controls (spike-in and hybridization controls) using Expression Console software (Affymetrix) and AffyQCReport (Gautier et al., 2004). An r^2 correlation value of 0.94 between biological replicates was used as a cutoff for reproducibility of the data. Probe sets that are annotated by The Arabidopsis Information Resource to hybridize to multiple loci in the *Arabidopsis* genome were removed from further analysis based on the affy_ATH1_array_elements-2010-12-20 table.

Salt-regulated differentially expressed probe sets were determined using LIMMA and EDGE packages in R (Smyth, 2005; Storey et al., 2005; Leek et al., 2006). P values were corrected for multiple testing using the Benjamini-Hochberg method, and probe sets were considered significantly differentially expressed if the P value $\leq$ 0.001 and expression differed by at least twofold between contrasting sample types. A 10% false discovery rate threshold was used in EDGE combined with a twofold change cutoff. Age-regulated probe sets were identified using LIMMA as described above except that a twofold change criteria was not used. The final list of NaCl-regulated probe sets was attained by combining the lists from LIMMA and EDGE and subtracting age-regulated probe sets on a per cell-type basis. For example, if a gene was identified as salt regulated in the STE layer and age regulated in the END layer, it would not be removed, while if it was also age regulated in the STE layer, it would be removed from further analysis.

A soft clustering algorithm, fuzzy C-means, was used to partition the significant differentially expressed genes based on their spatio-temporal expression patterns (Hathaway et al., 1996). A probability cutoff of 0.5 was chosen as this led to stringent clustering and assignment of each gene to only one cluster. Due to this stringency, some genes were not included in any cluster as they did not correlate strongly with any of the predominant patterns found. Different C values (number of clusters) were tested from 15 to 50. Enrichment of GO terms was used to evaluate each C value (Ashburner et al., 2000; Brady et al., 2007). Partitioning the data into 25 clusters led to the largest number of enriched GO categories with 3897 genes being clustered in total. GO category enrichment was performed using the ChipEnrich JAVA application (Brady et al., 2007).

Primer pairs were designed for six genes (At1g71000, At2g33380, At3g22570, At4g18430, At4g30460, and At5g66400) identified in the microarray to be regulated by NaCl in the EPI cell layer. The same RNA samples used for microarray analyses were used for cDNA synthesis and qRT-PCR. Quantitative RT-PCR was performed using three biological replicates on a 7900 HT real-time PCR System (Applied Biosystems) using Power SYBR Green chemistry (Applied Biosystems).

Development of an eFP Browser-Style Visualization Tool for the Spatio-Temporal Map

An eFP Web-based browser inspired by the work of Winter et al. (2007) was designed to display gene expression values obtained from the spatio-temporal map for salt stress. Gene expression values were unlog$_2$ transformed and visualized. A cartoon representation of the root was drawn and each quadrant given a defined color. For each gene queried, the maximum expression value was identified and drawn as red (255 red, 0 green, and 0 blue). The HEX color value for green was calculated for all other samples using the following formula: signal_sample * 255/maxSignal. A Web implementation of this eFP browser can be found at (http://dinnenylab.dpb.carnegiescience.edu).

Secondary Signaling Network Construction

Hormone treatment data sets were generated by the AtGenExpress consortium and described previously (Nemhauser et al., 2006). Original .cel files were downloaded from http://www.Arabidopsis.org/. Probe hybridization values were extracted and normalized using GCRMA (Irizarry et al., 2006). Pairwise comparisons were made between hormone-treated and control samples at each time point using LIMMA. Genes were ranked based on the B-statistic of differential expression, and the top 400 genes (number chosen empirically) with the highest values were chosen for further analysis. K-mean clustering was used to group genes into seven submodules using the city-block distance metric. Gene membership was compared between the salt stress clusters and the hormone submodules and the significance of shared membership calculated using the hypergeometric probability. P values were corrected for multiple testing by calculating their Q-values (Storey and Tibshirani, 2003). A network diagram illustrating the inferred secondary signaling network was visualized using Cytoscape (Shannon et al., 2003) and are available for viewing at (http://dinnenylab.dpb.carnegiescience.edu).

Quantitation of ABA Content

Seedlings were grown as described above for 5 d and transferred to medium containing 140 mM NaCl for varying lengths of time. The time of transfer was staggered so that samples were collected together at the same time of day. Whole roots were harvested and frozen in liquid nitrogen. ABA and associated metabolites were quantified from 500 mg of lyophilized tissue at the National Research Council Canada facility using high-performance liquid chromatography and tandem mass spectrometry. Three biological replicates were performed per sample type.

High-Throughput qRT-PCR

Col-0 and *aba2-sail* mutants were grown under standard conditions for 5 d, and seedlings were transferred to either standard or 140 mM NaCl-supplemented medium for 1, 3, or 32 h. Whole roots were harvested from three biological replicates. To characterize the role of tissue-specific ABA signaling, crosses were made between the *UAS:abi1-1* transgene and four different enhancer-trap lines (*J0951*, *J0571*, *Q2500*, and *Q0990*), and F1 seeds were collected. A control genotype was generated by crossing the *UAS:abi1-1* transgenic line to the C24 ecotype. Fifteen to 20 seedlings of the different transactivation lines were grown for 5 d and then transferred to standard or 140 mM NaCl-supplemented medium for 1 h. Root tips (meristem and elongation zones) were harvested for RNA extraction. Two to three technical replicates and two biological replicates were generated per sample type. Total RNA was purified using the RNeasy plant mini kit (Qiagen). Quality and quantity of each RNA sample were analyzed using a Nanodrop spectrophotometer. cDNA synthesis, template preamplification, sample and assay loading, and programs were performed as previously described (Duan et al., 2013). Primer sequences and information of the 94 test genes are listed in Supplemental Data Set 8 online. Two control genes, AT4G37830 (cytochrome c-oxidase) and AT3G07480 (electron carrier/iron-sulfur cluster binding), were used for data normalization. Statistical testing for differential gene expression was determined using a two-way ANOVA test for genotype-by-environment interactions using MeV (http://www.tm4.org/mev.html) with a multiple testing corrected P value threshold of 0.01. Statistical tests were performed using $-\Delta\Delta CT$ (cycle threshold) values. Expression values used to create heat map diagrams were calculated using the $2^{-\Delta\Delta CT}$ method assuming perfect amplification efficiency.

Fluorescence Microscopy and Image Analysis

Fluorol yellow staining was used to visualize suberin deposition during salt stress (Roppolo et al., 2011; Naseer et al., 2012). Roots were transferred to standard or salt stress medium, and the positions of the root tips were marked. After 24 h of growth, roots were cut at the position where the root tip originally was at the point of transfer and tissue was stained with Fluorol yellow 088 as previously described (Lux et al., 2005). The average fluorescence intensity of a cut proximal region was measured with ImageJ. Images were quantified for seven roots grown transferred to

standard conditions and 11 roots transferred to medium supplemented with 140 mM NaCl.

To monitor dynamic changes in ABA signaling in primary roots, fluorescence of the *ProRAB18:GFP* reporter was imaged on a Leica fluorescence dissecting microscope during treatment. GFP fluorescence intensity at each time point was quantified using ImageJ. The fluorescence intensity of a 5124 pixels area in the early maturation zone was measured for each root. The starting point of the early maturation zone was defined by the initiation of root hairs. Fluorescence intensity was subtracted from the background signal, which was measured in the same way. Fluorescence was quantified for five roots.

For quantification of *ProRGA:GFP:RGA* levels, GFP fluorescence intensity was quantified from a maximum projection of a z-stack of images taken of the meristem from the epidermis to the medial plane of the root. The mean background intensity was subtracted from each measurement. Ten roots were used for each condition, and the average was calculated.

To quantify changes in BZR1-YFP nuclear accumulation, the elongation zone of 5 to 6 d postgermination seedlings was imaged on a Leica SP5 confocal microscope using a ×63 lens. The starting point of the elongation zone was defined by cell shape (length to width ratio greater than one). There were nine to 16 cells in the epidermis per root that were in the elongation zone. The fluorescence intensity of the nucleus was measured at its greatest diameter using ImageJ and the measurements from one root averaged together. The experiment was performed three times with three to four seedlings quantified for each time point and treatment. The standard error of the mean shows the variation between different replicates. For all imaging experiments, a two-tailed Student's t test was used to calculate statistical significance and a threshold P value < 0.05 was used.

Accession Numbers

All microarray data generated for this study were deposited in the Gene Expression Omnibus under accession numbers GSE46205 and GSE46208. Gene IDs for genes used for real-time quantitative PCR can be found in Supplemental Data Set 8 online. Supplemental Data Sets 1 to 8 online are deposited in the DRYAD repository: http://dx.doi.org/10.5061/dryad.6g2g2.

Supplemental Data

The following materials are available in the online version of this article.

Supplemental Figure 1. Time-Lapse Imaging System and Semi-automated Image Analysis.

Supplemental Figure 2. Gene Ontology Annotation Enrichment in Genes Expressed during the Salt Stress Response in Whole Roots.

Supplemental Figure 3. Expression of GFP Reporter Lines Used for FACS after Prolonged Salt Treatment.

Supplemental Figure 4. Percent Enrichment of GFP-Expressing Cells after FACS Isolation from Protoplasted *ProWER:erGFP* Roots.

Supplemental Figure 5. Comparison of Gene Expression Profiles for Six Genes Using qRT-PCR or Microarray-Based Quantitation.

Supplemental Figure 6. Expression Pattern of Genes in the Spatio-Temporal Salt Response Data Set with Known Tissue-Specific Expression in Roots.

Supplemental Figure 7. Salt-Responsive Genes Show Cell Type–Specific Changes in Expression throughout the Time Course.

Supplemental Figure 8. Fluorol Yellow Staining Shows an Enrichment of Suberin Deposition during the Salt Response; the *aba2-sail* Allele Is an RNA Null.

Supplemental Figure 9. The *ProRAB18:GFP* Reporter Is Activated Briefly in the Early Maturation Zone of the Root.

Supplemental Figure 10. Inferred Expression Pattern for JA and BR Pathway-Associated Genes.

Supplemental Table 1. Time Table of Salt Treatments for FACS Isolation of Cell Types after Salt Treatment.

Supplemental Movie 1. Example of Output for the Computational Algorithm Used to Quantify Root Growth Rates.

Supplemental Movie 2. Time-Lapse Movie of Primary Root Growth after Transfer to Standard or 140 mM NaCl Supplemented Medium.

Supplemental Data Set 1. Average Relative Root Growth Rates and Raw Data from Time-Lapse Imaging.

Supplemental Data Set 2. Microarray Data and Analysis of Gene Expression in Whole Roots Treated with Salt Stress for 1 h to 8 d.

Supplemental Data Set 3. Microarray Quantitation of Gene Expression for FACS-Isolated Cells after Treatment of Roots with Salt Stress for 1 h to 2 d.

Supplemental Data Set 4. Significant Differentially Expressed Genes Identified in the Spatio-Temporal Gene Expression Map Using LIMMA or EDGE.

Supplemental Data Set 5. Salt Stress–Responsive Clusters and GO Term Enrichment.

Supplemental Data Set 6. Hormone Submodules and the Secondary Signaling Network.

Supplemental Data Set 7. *BZR1* Target Genes Regulated by Salt Stress.

Supplemental Data Set 8. Oligonucleotides Used in This Study for High-Throughput qRT-PCR Experiments.

AUTHOR CONTRIBUTIONS

Y.G., R.W., C.W.W., F.X., and J.R.D. conceived and designed the study. Y.G., R.W., C.W.W., F.X., P.M.Y.C., C.T., and L.D. performed all experiments. Y.G., R.W., C.W.W., F.X., X.W., and J.R.D. performed all the analyses. X.W. wrote all computational algorithms original to this work. Y.G., R.W., and J.R.D. wrote the article.

REFERENCES

Abramoff, M.D., Magelhaes, P.J., and Ram, S.J. (2004). Image processing with ImageJ. Biophotonics International **11:** 36–42.

Achard, P., Cheng, H., De Grauwe, L., Decat, J., Schoutteten, H., Moritz, T., Van Der Straeten, D., Peng, J., and Harberd, N.P. (2006). Integration of plant responses to environmentally activated phytohormonal signals. Science **311:** 91–94.

Antoni, R., Gonzalez-Guzman, M., Rodriguez, L., Peirats-Llobet, M., Pizzio, G.A., Fernandez, M.A., De Winne, N., De Jaeger, G., Dietrich, D., Bennett, M.J., and Rodriguez, P.L. (2013). PYRABACTIN RESISTANCE1-LIKE8 plays an important role for the regulation of abscisic acid signaling in root. Plant Physiol. **161:** 931–941.

Arioli, T., et al. (1998). Molecular analysis of cellulose biosynthesis in *Arabidopsis*. Science **279:** 717–720.

Ashburner, M., et al; The Gene Ontology Consortium (2000). Gene ontology: Tool for the unification of biology. Nat. Genet. **25:** 25–29.

Bai, M.Y., Shang, J.X., Oh, E., Fan, M., Bai, Y., Zentella, R., Sun, T.P., and Wang, Z.Y. (2012). Brassinosteroid, gibberellin and phytochrome impinge on a common transcription module in *Arabidopsis*. Nat. Cell Biol. **14:** 810–817.

Birnbaum, K., Jung, J.W., Wang, J.Y., Lambert, G.M., Hirst, J.A., Galbraith, D.W., and Benfey, P.N. (2005). Cell type-specific expression profiling in plants via cell sorting of protoplasts from fluorescent reporter lines. Nat. Methods **2:** 615–619.

Birnbaum, K., Shasha, D.E., Wang, J.Y., Jung, J.W., Lambert, G.M., Galbraith, D.W., and Benfey, P.N. (2003). A gene expression map of the *Arabidopsis* root. Science **302:** 1956–1960.

Brady, S.M., Orlando, D.A., Lee, J.Y., Wang, J.Y., Koch, J., Dinneny, J.R., Mace, D., Ohler, U., and Benfey, P.N. (2007). A high-resolution root spatiotemporal map reveals dominant expression patterns. Science **318:** 801–806.

Breakfield, N.W., Corcoran, D.L., Petricka, J.J., Shen, J., Sae-Seaw, J., Rubio-Somoza, I., Weigel, D., Ohler, U., and Benfey, P.N. (2012). High-resolution experimental and computational profiling of tissue-specific known and novel miRNAs in *Arabidopsis*. Genome Res. **22:** 163–176.

Brooks, T.L., Miller, N.D., and Spalding, E.P. (2010). Plasticity of *Arabidopsis* root gravitropism throughout a multidimensional condition space quantified by automated image analysis. Plant Physiol. **152:** 206–216.

Chen, Q., et al. (2011). The basic helix-loop-helix transcription factor MYC2 directly represses *PLETHORA* expression during jasmonate-mediated modulation of the root stem cell niche in *Arabidopsis*. Plant Cell **23:** 3335–3352.

Chini, A., Fonseca, S., Fernández, G., Adie, B., Chico, J.M., Lorenzo, O., García-Casado, G., López-Vidriero, I., Lozano, F.M., Ponce, M.R., Micol, J.L., and Solano, R. (2007). The JAZ family of repressors is the missing link in jasmonate signalling. Nature **448:** 666–671.

Deal, R.B., and Henikoff, S. (2010). A simple method for gene expression and chromatin profiling of individual cell types within a tissue. Dev. Cell **18:** 1030–1040.

Deal, R.B., and Henikoff, S. (2011). The INTACT method for cell type-specific gene expression and chromatin profiling in *Arabidopsis thaliana*. Nat. Protoc. **6:** 56–68.

Dinneny, J.R. (2010). Analysis of the salt-stress response at cell-type resolution. Plant Cell Environ. **33:** 543–551.

Dinneny, J.R. (2013). Cell-type resolution analysis of root development and environmental responses. In Root Genomics and Soil Interactions, M.D. Crespi, ed (Ames, Iowa: John Wiley & Sons), pp. 63–78.

Dinneny, J.R., and Benfey, P.N. (2009). Studying root development using a genomic approach. In Annual Plant Reviews: Root Development, Vol. 37, T. Beeckman, ed (Oxford, UK: Wiley-Blackwell),.

Dinneny, J.R., Long, T.A., Wang, J.Y., Jung, J.W., Mace, D., Pointer, S., Barron, C., Brady, S.M., Schiefelbein, J., and Benfey, P.N. (2008). Cell identity mediates the response of *Arabidopsis* roots to abiotic stress. Science **320:** 942–945.

Duan, L., Dietrich, D., Ng, C.H., Chan, P.M., Bhalerao, R., Bennett, M.J., and Dinneny, J.R. (2013). Endodermal ABA signaling promotes lateral root quiescence during salt stress in *Arabidopsis* seedlings. Plant Cell **25:** 324–341.

Finkelstein, R.R., and Rock, C.D. (2002). Abscisic acid biosynthesis and response. Arabidopsis Book **1:** e0058.

Flowers, T.J., Garcia, A., Koyama, M., and Yeo, A.R. (1997). Breeding for salt tolerance in crop plants- The role of molecular biology. Acta Physiol. Plant. **19:** 427–433.

Fujii, H., Chinnusamy, V., Rodrigues, A., Rubio, S., Antoni, R., Park, S.Y., Cutler, S.R., Sheen, J., Rodríguez, P.L., and Zhu, J.K. (2009). In vitro reconstitution of an abscisic acid signalling pathway. Nature **462:** 660–664.

Fujita, Y., Fujita, M., Shinozaki, K., and Yamaguchi-Shinozaki, K. (2011). ABA-mediated transcriptional regulation in response to osmotic stress in plants. J. Plant Res. **124:** 509–525.

Gallego-Bartolomé, J., Minguet, E.G., Grau-Enguix, F., Abbas, M., Locascio, A., Thomas, S.G., Alabadí, D., and Blázquez, M.A. (2012). Molecular mechanism for the interaction between gibberellin and brassinosteroid signaling pathways in *Arabidopsis*. Proc. Natl. Acad. Sci. USA **109:** 13446–13451.

Gautier, L., Cope, L., Bolstad, B.M., and Irizarry, R.A. (2004). affy—Analysis of Affymetrix GeneChip data at the probe level. Bioinformatics **20:** 307–315.

Gifford, M.L., Dean, A., Gutiérrez, R.A., Coruzzi, G.M., and Birnbaum, K.D. (2008). Cell-specific nitrogen responses mediate developmental plasticity. Proc. Natl. Acad. Sci. USA **105:** 803–808.

Giraudat, J., Hauge, B.M., Valon, C., Smalle, J., Parcy, F., and Goodman, H.M. (1992). Isolation of the *Arabidopsis ABI3* gene by positional cloning. Plant Cell **4:** 1251–1261.

González-Guzmán, M., Apostolova, N., Bellés, J.M., Barrero, J.M., Piqueras, P., Ponce, M.R., Micol, J.L., Serrano, R., and Rodríguez, P.L. (2002). The short-chain alcohol dehydrogenase ABA2 catalyzes the conversion of xanthoxin to abscisic aldehyde. Plant Cell **14:** 1833–1846.

González-Guzman, M., Pizzio, G.A., Antoni, R., Vera-Sirera, F., Merilo, E., Bassel, G.W., Fernández, M.A., Holdsworth, M.J., Perez-Amador, M.A., Kollist, H., and Rodríguez, P.L. (2012). *Arabidopsis* PYR/PYL/RCAR receptors play a major role in quantitative regulation of stomatal aperture and transcriptional response to abscisic acid. Plant Cell **24:** 2483–2496.

Hathaway, R.J., Bezdek, J.C., and Pal, N.R. (1996). Sequential competitive learning and the Fuzzy c-Means clustering algorithms. Neural Netw. **9:** 787–796.

He, J.X., Gendron, J.M., Sun, Y., Gampala, S.S., Gendron, N., Sun, C.Q., and Wang, Z.Y. (2005). BZR1 is a transcriptional repressor with dual roles in brassinosteroid homeostasis and growth responses. Science **307:** 1634–1638.

Helariutta, Y., Fukaki, H., Wysocka-Diller, J., Nakajima, K., Jung, J., Sena, G., Hauser, M.T., and Benfey, P.N. (2000). The *SHORT-ROOT* gene controls radial patterning of the *Arabidopsis* root through radial signaling. Cell **101:** 555–567.

Irizarry, R.A., Wu, Z., and Jaffee, H.A. (2006). Comparison of Affymetrix GeneChip expression measures. Bioinformatics **22:** 789–794.

Iuchi, S., Kobayashi, M., Taji, T., Naramoto, M., Seki, M., Kato, T., Tabata, S., Kakubari, Y., Yamaguchi-Shinozaki, K., and Shinozaki, K. (2001). Regulation of drought tolerance by gene manipulation of 9-*cis*-epoxycarotenoid dioxygenase, a key enzyme in abscisic acid biosynthesis in *Arabidopsis*. Plant J. **27:** 325–333.

Iyer-Pascuzzi, A.S., Jackson, T., Cui, H., Petricka, J.J., Busch, W., Tsukagoshi, H., and Benfey, P.N. (2011). Cell identity regulators

link development and stress responses in the *Arabidopsis* root. Dev. Cell **21:** 770–782.

Karahara, I., Ikeda, A., Kondo, T., and Uetake, Y. (2004). Development of the Casparian strip in primary roots of maize under salt stress. Planta **219:** 41–47.

Kilian, J., Whitehead, D., Horak, J., Wanke, D., Weinl, S., Batistic, O., D'Angelo, C., Bornberg-Bauer, E., Kudla, J., and Harter, K. (2007). The AtGenExpress global stress expression data set: Protocols, evaluation and model data analysis of UV-B light, drought and cold stress responses. Plant J. **50:** 347–363.

Kim, T.H., et al. (2011). Chemical genetics reveals negative regulation of abscisic acid signaling by a plant immune response pathway. Curr. Biol. **21:** 990–997.

Kushiro, T., Okamoto, M., Nakabayashi, K., Yamagishi, K., Kitamura, S., Asami, T., Hirai, N., Koshiba, T., Kamiya, Y., and Nambara, E. (2004). The *Arabidopsis* cytochrome P450 CYP707A encodes ABA 8'-hydroxylases: Key enzymes in ABA catabolism. EMBO J. **23:** 1647–1656.

Lee, J.Y., Colinas, J., Wang, J.Y., Mace, D., Ohler, U., and Benfey, P.N. (2006). Transcriptional and posttranscriptional regulation of transcription factor expression in *Arabidopsis* roots. Proc. Natl. Acad. Sci. USA **103:** 6055–6060.

Lee, M.M., and Schiefelbein, J. (1999). WEREWOLF, a MYB-related protein in *Arabidopsis*, is a position-dependent regulator of epidermal cell patterning. Cell **99:** 473–483.

Leek, J.T., Monsen, E., Dabney, A.R., and Storey, J.D. (2006). EDGE: Extraction and analysis of differential gene expression. Bioinformatics **22:** 507–508.

Lux, A., Morita, S., Abe, J., and Ito, K. (2005). An improved method for clearing and staining free-hand sections and whole-mount samples. Ann. Bot. (Lond.) **96:** 989–996.

Ma, Y., Szostkiewicz, I., Korte, A., Moes, D., Yang, Y., Christmann, A., and Grill, E. (2009). Regulators of PP2C phosphatase activity function as abscisic acid sensors. Science **324:** 1064–1068.

Miller, N.D., Parks, B.M., and Spalding, E.P. (2007). Computer-vision analysis of seedling responses to light and gravity. Plant J. **52:** 374–381.

Munns, R. (2002). Comparative physiology of salt and water stress. Plant Cell Environ. **25:** 239–250.

Mustroph, A., Juntawong, P., and Bailey-Serres, J. (2009). Isolation of plant polysomal mRNA by differential centrifugation and ribosome immunopurification methods. Methods Mol. Biol. **553:** 109–126.

Naseer, S., Lee, Y., Lapierre, C., Franke, R., Nawrath, C., and Geldner, N. (2012). Casparian strip diffusion barrier in *Arabidopsis* is made of a lignin polymer without suberin. Proc. Natl. Acad. Sci. USA **109:** 10101–10106.

Nawy, T., Lee, J.Y., Colinas, J., Wang, J.Y., Thongrod, S.C., Malamy, J.E., Birnbaum, K., and Benfey, P.N. (2005). Transcriptional profile of the *Arabidopsis* root quiescent center. Plant Cell **17:** 1908–1925.

Nemhauser, J.L., Hong, F., and Chory, J. (2006). Different plant hormones regulate similar processes through largely nonoverlapping transcriptional responses. Cell **126:** 467–475.

Noguchi, T., Fujioka, S., Choe, S., Takatsuto, S., Yoshida, S., Yuan, H., Feldmann, K.A., and Tax, F.E. (1999). Brassinosteroid-insensitive dwarf mutants of *Arabidopsis* accumulate brassinosteroids. Plant Physiol. **121:** 743–752.

Oh, E., Zhu, J.Y., and Wang, Z.Y. (2012). Interaction between BZR1 and PIF4 integrates brassinosteroid and environmental responses. Nat. Cell Biol. **14:** 802–809.

Park, S.Y., et al. (2009). Abscisic acid inhibits type 2C protein phosphatases via the PYR/PYL family of START proteins. Science **324:** 1068–1071.

Passioura, J.B., and Munns, R. (2000). Rapid environmental changes that affect leaf water status induce transient surges and pauses in leaf expansion rate. Aust. J. Plant Physiol. **27:** 941–948.

Petersson, S.V., Johansson, A.I., Kowalczyk, M., Makoveychuk, A., Wang, J.Y., Moritz, T., Grebe, M., Benfey, P.N., Sandberg, G., and Ljung, K. (2009). An auxin gradient and maximum in the *Arabidopsis* root apex shown by high-resolution cell-specific analysis of IAA distribution and synthesis. Plant Cell **21:** 1659–1668.

Petricka, J.J., Schauer, M.A., Megraw, M., Breakfield, N.W., Thompson, J.W., Georgiev, S., Soderblom, E.J., Ohler, U., Moseley, M.A., Grossniklaus, U., and Benfey, P.N. (2012). The protein expression landscape of the *Arabidopsis* root. Proc. Natl. Acad. Sci. USA **109:** 6811–6818.

Rademacher, W. (2000). Growth retardants: Effects on gibberellin biosynthesis and other metabolic pathways. Annu. Rev. Plant Physiol. Plant Mol. Biol. **51:** 501–531.

Reddy, G.V., Gordon, S.P., and Meyerowitz, E.M. (2007). Unravelling developmental dynamics: Transient intervention and live imaging in plants. Nat. Rev. Mol. Cell Biol. **8:** 491–501.

Rodríguez, H.G., Roberts, J., Jordan, W.R., and Drew, M.C. (1997). Growth, water relations, and accumulation of organic and inorganic solutes in roots of maize seedlings during salt stress. Plant Physiol. **113:** 881–893.

Rogers, E.D., Jackson, T., Moussaieff, A., Aharoni, A., and Benfey, P.N. (2012). Cell type-specific transcriptional profiling: Implications for metabolite profiling. Plant J. **70:** 5–17.

Roppolo, D., De Rybel, B., Tendon, V.D., Pfister, A., Alassimone, J., Vermeer, J.E., Yamazaki, M., Stierhof, Y.D., Beeckman, T., and Geldner, N. (2011). A novel protein family mediates Casparian strip formation in the endodermis. Nature **473:** 380–383.

Sabatini, S., Heidstra, R., Wildwater, M., and Scheres, B. (2003). *SCARECROW* is involved in positioning the stem cell niche in the *Arabidopsis* root meristem. Genes Dev. **17:** 354–358.

Saito, S., Hirai, N., Matsumoto, C., Ohigashi, H., Ohta, D., Sakata, K., and Mizutani, M. (2004). *Arabidopsis* CYP707As encode (+)-abscisic acid 8'-hydroxylase, a key enzyme in the oxidative catabolism of abscisic acid. Plant Physiol. **134:** 1439–1449.

Schaller, G.E., and Kieber, J.J. (2002). Ethylene. Arabidopsis Book **1:** e0071.

Scheres, B., Benfey, P., and Dolan, L. (2002). Root development. Arabidopsis Book **1:** e0101.

Shannon, P., Markiel, A., Ozier, O., Baliga, N.S., Wang, J.T., Ramage, D., Amin, N., Schwikowski, B., and Ideker, T. (2003). Cytoscape: A software environment for integrated models of biomolecular interaction networks. Genome Res. **13:** 2498–2504.

Sharp, R.E., and LeNoble, M.E. (2002). ABA, ethylene and the control of shoot and root growth under water stress. J. Exp. Bot. **53:** 33–37.

Sharp, R.E., LeNoble, M.E., Else, M.A., Thorne, E.T., and Gherardi, F. (2000). Endogenous ABA maintains shoot growth in tomato independently of effects on plant water balance: Evidence for an interaction with ethylene. J. Exp. Bot. **51:** 1575–1584.

Skirycz, A., Claeys, H., De Bodt, S., Oikawa, A., Shinoda, S., Andriankaja, M., Maleux, K., Eloy, N.B., Coppens, F., Yoo, S.D., Saito, K., and Inzé, D. (2011). Pause-and-stop: the effects of osmotic stress on cell proliferation during early leaf development in *Arabidopsis* and a role for ethylene signaling in cell cycle arrest. Plant Cell **23:** 1876–1888.

Skirycz, A., De Bodt, S., Obata, T., De Clercq, I., Claeys, H., De Rycke, R., Andriankaja, M., Van Aken, O., Van Breusegem, F., Fernie, A.R., and Inzé, D. (2010). Developmental stage specificity and the role of mitochondrial metabolism in the response of *Arabidopsis* leaves to prolonged mild osmotic stress. Plant Physiol. **152:** 226–244.

Smyth, G.K. (2005). Limma: Linear models for microarray data. In Bioinformatics and Computational Biology Solutions Using R and Bioconductor, R. Gentleman, V. Carey, S. Dudoit, R. Irizarry, and W. Huber, eds (New York: Springer), pp. 397–420.

Sozzani, R., Cui, H., Moreno-Risueno, M.A., Busch, W., Van Norman, J.M., Vernoux, T., Brady, S.M., Dewitte, W., Murray, J.A., and Benfey, P.N. (2010). Spatiotemporal regulation of cell-cycle genes by SHORTROOT links patterning and growth. Nature **466:** 128–132.

Spollen, W.G., LeNoble, M.E., Samuels, T.D., Bernstein, N., and Sharp, R.E. (2000). Abscisic acid accumulation maintains maize primary root elongation at low water potentials by restricting ethylene production. Plant Physiol. **122:** 967–976.

Storey, J.D., and Tibshirani, R. (2003). Statistical significance for genomewide studies. Proc. Natl. Acad. Sci. USA **100:** 9440–9445.

Storey, J.D., Xiao, W., Leek, J.T., Tompkins, R.G., and Davis, R.W. (2005). Significance analysis of time course microarray experiments. Proc. Natl. Acad. Sci. USA **102:** 12837–12842.

Tan, B.C., Joseph, L.M., Deng, W.T., Liu, L., Li, Q.B., Cline, K., and McCarty, D.R. (2003). Molecular characterization of the *Arabidopsis* 9-*cis* epoxycarotenoid dioxygenase gene family. Plant J. **35:** 44–56.

Tsukagoshi, H., Busch, W., and Benfey, P.N. (2010). Transcriptional regulation of ROS controls transition from proliferation to differentiation in the root. Cell **143:** 606–616.

Tyler, L., Thomas, S.G., Hu, J., Dill, A., Alonso, J.M., Ecker, J.R., and Sun, T.P. (2004). Della proteins and gibberellin-regulated seed germination and floral development in *Arabidopsis*. Plant Physiol. **135:** 1008–1019.

Wang, Z.Y., Nakano, T., Gendron, J., He, J., Chen, M., Vafeados, D., Yang, Y., Fujioka, S., Yoshida, S., Asami, T., and Chory, J. (2002). Nuclear-localized BZR1 mediates brassinosteroid-induced growth and feedback suppression of brassinosteroid biosynthesis. Dev. Cell **2:** 505–513.

Wee, C.W., and Dinneny, J.R. (2010). Tools for high-spatial and temporal-resolution analysis of environmental responses in plants. Biotechnol. Lett. **32:** 1361–1371.

Winter, D., Vinegar, B., Nahal, H., Ammar, R., Wilson, G.V., and Provart, N.J. (2007). An "Electronic Fluorescent Pictograph" browser for exploring and analyzing large-scale biological data sets. PLoS ONE **2:** e718.

Wu, G., Cameron, J.N., Ljung, K., and Spalding, E.P. (2010). A role for ABCB19-mediated polar auxin transport in seedling photomorphogenesis mediated by cryptochrome 1 and phytochrome B. Plant J. **62:** 179–191.

Xi, W., Liu, C., Hou, X., and Yu, H. (2010). *MOTHER OF FT AND TFL1* regulates seed germination through a negative feedback loop modulating ABA signaling in *Arabidopsis*. Plant Cell **22:** 1733–1748.

Xiong, L., and Zhu, J.K. (2002). Salt tolerance. The Arabidopsis Book **1:** e0048, doi/10.1199/tab.0048.

Zhu, J.K. (2002). Salt and drought stress signal transduction in plants. Annu. Rev. Plant Biol. **53:** 247–273.